An-Najah National University
Faculty of Engineering and IT

جامعة النجاح الوطنية
كلية الهندسة وتكنولوجيا المعلومات

GSM based non-invasive glucose monitoring system base on NIR spectroscopy and Microstrip resonator

2023-2024

Electrical Engineering

Muhammad Danoun 11820461

Anas Ali 11820151

Supervisor: Dr. Omar Tamimi

الإهداء:

قال تعالى: {قُلْ هَلْ يَسْتَوِي الَّذِينَ يَعْلَمُونَ وَالَّذِينَ لَا يَعْلَمُونَ...}

إلى كل من ساندنا

ورسموا لنا طريق العلم والمعرفة...

الحمد لله حمداً كثيراً أن منَّ علينا بنعمة العقل والإدراك، وأرشد الإنسان إلى ما فيه الخيرَ والصلاح، ونسأل الله سبحانه وتعالى الهداية في الدنيا والآخرة...

بعد الحمد و الشكر نتوجه بإهداء رسالتنا بداية الى شعبنا في غزة الذي ضحى بالغالي و النفيس في سبيل ديننا و وطننا ونسال الله ان يرحم شهداءنا و يعافي جرحانا ثم الى كل من سار معنا منذ بداية الطريق و صبر علينا و تحمل المشقة لأجلنا، خير سند و أوفى صحبة و أحن خلق الله، الى أمهاتنا وآباءنا وإخواننا وأحبابنا نقول جزاكم الله بما صابرت في الدارين و نسأل الله أن نكون دوماً عند حسن ظنكم، ثم الشكر موصول لمن وقف معنا و ساندنا خلال مسيرتنا التعليمية من أساتذة و مشرفين كل باسمه و لقبه و الشكر موصول للدكتور عمر التميمي الذي كان معنا لحظة بلحظة حتى وفقنا الله بإنجازه، فجزاه الله خير الجزاء...

أهلنا ومعلمينا ومرشدينا وكل من له حقّ ع علينا...

لقد أتممنا إنجاز البحث العلمي المتعلق بمشروع التخرج لإتمام مرحلة البكالوريوس من جامعة النجاح الوطنية_ نابلس

الشكر والإهداء موجه أيضاً إلى طاقم عمل كلية الهندسة وتكنولوجيا المعلومات بما فيها السادة عميد الكلية ورئيس قسم الهندسة الكهربائية والأكاديميين ومشرفي المختبرات ونسأل الله سبحانه وتعالى أن يكتب لنا خير ما في هذا البحث.

فإليكم نهدي هذا العمل المتواضع

أما بعد...

Abstract:

In the wake of the increasing global diabetic population, there's been a surge in the affliction of individuals facing discomfort and infections due to the invasive techniques employed by conventional commercial glucose meters. The pursuit of non-invasive blood glucose monitoring has emerged as a pivotal area of global research, promising respite to countless patients. Addressing this crucial need, we propose an inventive approach that melds Near-Infrared (NIR) spectroscopy with Microstrip resonators, seamlessly integrating them into a GSM-based monitoring system designed for assessing glucose levels without the need for invasive methods.

Objectives of the Study:

Development of Non-Invasive Monitoring Technology: Design and implement a robust system capable of non-invasively monitoring blood glucose levels using NIR spectroscopy integrated with Microstrip resonator technology.

Real-Time Data Transmission: Establish a seamless data transmission system utilizing GSM technology, enabling real-time monitoring and analysis of glucose levels remotely.

Accuracy and Reliability Assessment: Conduct comprehensive testing and validation procedures to ensure the accuracy, reliability, and safety of the developed non-invasive monitoring system in diverse scenarios and conditions.

User-Friendly Interface: Develop a user-friendly interface for easy interaction and interpretation of glucose level data, promoting usability for both patients and healthcare professionals.

Diabetes Overview:

Diabetes is classified based on blood sugar levels. Glucose, derived from our diet, transforms into adenosine triphosphate (ATP) in cell mitochondria, providing essential energy. After eating, blood sugar rises, stimulating insulin production in the pancreas. Insulin facilitates glucose entry into cells, crucial for preventing diabetes.

Contents

Chapter1:

Introduction

1.1. Overview of Diabetes:

Diabetes stands as one of the prevailing chronic ailments affecting human populations globally. It stems primarily from genetic predispositions, immune system dysregulation, and other influencing factors that lead to a decline in body functionality, insulin resistance, and imbalanced glucose levels in the body. This metabolic imbalance results in impaired glucose metabolism and the onset of hyperglycemia. Diabetes segregates into two main types: type 1 and type 2. Type 1 diabetes arises due to insufficient insulin secretion from the pancreas, while type 2 occurs largely due to ineffective insulin utilization resulting from decreased insulin sensitivity and insulin resistance in patients. The condition carries a high incidence rate, leads to numerous complications, has multifaceted causative factors, proves challenging to cure, and poses severe health risks. As a consequence, various fields have actively engaged in diabetes research. More than 90% of diabetes cases are type 2, and estimations from the International Diabetes Federation indicate a steep rise in the global diabetic population. The World Health Organization (WHO) reports approximately 450 million diabetes cases worldwide, potentially surging to 700 million by 2045. By 2030 and 2060, the United States alone may witness increases to 39.7 million and 60.6 million cases, respectively. Besides diagnosed cases, a substantial portion of the population remains undiagnosed or at significant risk, intensifying the focus on diabetes prevention, particularly in developed nations. Diagnosis and treatment of diabetes hold significant practical and economic significance. Glucose serves as the primary energy source for cell metabolism in the human body and is present not only in blood but also in intracellular fluids, interstitial fluids (ISF), tears, saliva, and urine. Presently, blood glucose concentration serves as the primary diagnostic criterion, with WHO standards setting fasting blood glucose (FBG) for normal individuals between 3.9–6.1mM and post-meal blood glucose at 7.8 mM or lower. Diagnosing diabetes is based on symptoms and specific blood glucose levels. Additionally, hypoglycemia, where blood glucose falls below 3.9 mM and lasts over 5 minutes, presents significant risks, particularly among elderly patients. Traditional blood glucose detection methods struggle to monitor nocturnal hypoglycemia timely, potentially escalating risks. Continuous Glucose Monitoring (CGM) holds promising clinical value and aligns more closely with market trends, especially in maintaining strict blood glucose control without increasing hypoglycemic risks.

1.2. Methods for Monitoring Blood Glucose Concentration:

According to whether the blood glucose test has caused injury to human skin, it can be simply divided into invasive and non-invasive blood glucose monitoring.

1.2.1. Invasive Blood Glucose Monitoring At present:

The prevailing method for blood glucose detection remains invasive, relying on blood sampling followed by in vitro analysis for glucose measurement. This approach, adopted in both medical facilities and household glucometers, involves drawing blood from subjects, typically on an empty stomach, to accurately measure blood glucose concentration using automatic biochemical analyzers in hospitals.

While precise, this method isn't conducive to continuous monitoring due to its cumbersome process, prolonged detection time, and substantial venous blood extraction. Self-monitoring of blood glucose (SMBG) involves checking blood glucose concentration at specific moments, often facilitated by home electronic glucose meters.

Household glucose meters commonly utilize glucose oxidase biosensors, analyzing fingertip blood with disposable paper strips to ascertain blood glucose concentration through chemical reaction currents. Commercial glycemic meter brands like Roche, Sano, Omron, Johnson and Johnson, Bayer, Abbott, Echeng, and Ecco are portable, cost-effective, easy to operate, and offer relatively accurate data, making them widely used at home. However, their downsides are notable.

Frequent blood collection from fingertips leads to deep punctures and slow wound healing, elevating infection risks and causing substantial pain and stress. Additionally, the disposable nature of test strips and blood needles incurs significant costs, particularly in underdeveloped regions.

The strips have a limited shelf life, and improper storage compromises the accuracy of blood glucose detection. Healthcare guidelines recommend SMBG four times daily, increasing to ten during illness or poor control, yet reports indicate that a significant portion of diabetics don't comply.

Timely insulin injections are crucial, as failure may lead to severe complications like diabetic ketoacidosis, cardiovascular diseases, blindness, stroke, and neurasthenia. Excessive insulin treatment poses risks of sudden drastic drops in blood glucose, potentially resulting in seizures, coma, or fatality. Clearly, the current SMBG method causes discomfort for patients and warrants improvement.

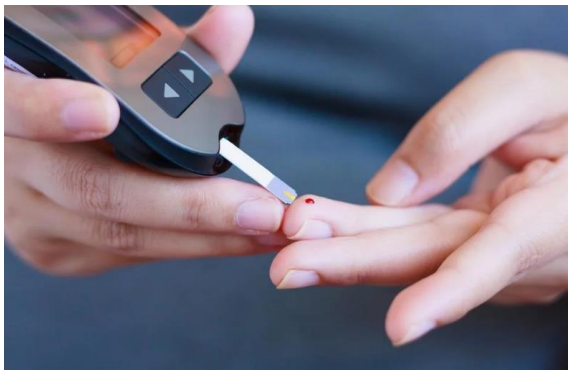

Figure1-1: Invasive Blood Glucose Monitoring

1.2.2. Non-Invasive Blood Glucose Monitoring:

Non-invasive blood glucose monitoring, as its name implies, refers to the detection of human blood glucose without causing damage to human tissues. There are lots of methods for non-invasive blood glucose detection, which can be generally divided into optical methods, microwave methods and electrochemical methods.

Optical methods include near-infrared reflectance spectroscopy (NIRS), polarized optical rotation, Raman spectroscopy, fluorescence, optical coherence tomography (OCT) and so on. in addition to glucose in human blood, there are also considerable amounts of glucose in other biofluids (such as saliva, tears, sweat, and Interstitial Fluid (ISF)).

Utilizing the coherent correlation between biofluids and blood glucose value, the electrochemical method usually measures the glucose content in body fluids first and obtains the blood glucose value indirectly after the calibration of the algorithm or data model.

The range of glucose in ISF is the closest to the range of blood glucose in both healthy and diabetic, which provides a theoretical basis for the development of an ISF glucose sensor. Trans dermal biofluid extraction generally adopts reverse iontophoresis (RI) technology, which can achieve the purpose of rapid extraction of ISF.

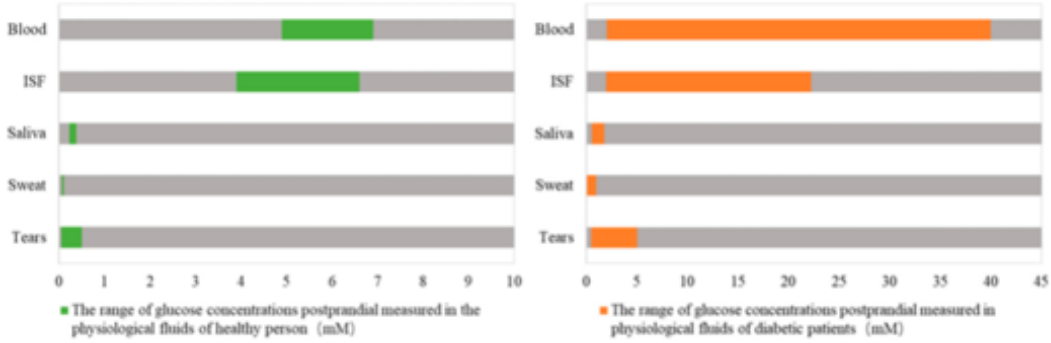

Figure1-2: Contrast of glucose concentrations in different physiological fluids between healthy and diabetic people.

This study primarily focuses on custom designing an optical glucose sensor incorporating light sources and detectors operating within the near-infrared (NIR) spectrum and Microstrip resonators. In near-infrared (NIR) spectrum extensive analysis of optimal light wavelengths is conducted to precisely determine glucose concentrations in solutions. The intensity of the signal transmitted through the sample relies on light absorption and scattering within the sample, characteristics influenced by the glucose concentration in the solution. The preference for using light sources within the VIS-NIR range over mid-infrared (MIR) sources stems from the lower absorption of VIS-NIR light by tissue and blood water content.

The strong absorption of MIR light by water diminishes the intensity of light capable of penetrating blood and tissue samples, limiting its detection capability. Unlike MIR light, VIS-NIR light can penetrate deeper into tissues, interacting with glucose molecules in both interstitial fluid and blood vessels. Although glucose diffuses from blood vessels into interstitial fluid over time, resulting in varying glucose levels between them, VIS-NIR light can instantaneously interact with glucose molecules in the blood, enhancing the sensor's sensitivity to real-time glucose concentration changes. Consequently, this study concentrates on VIS-NIR light sources.

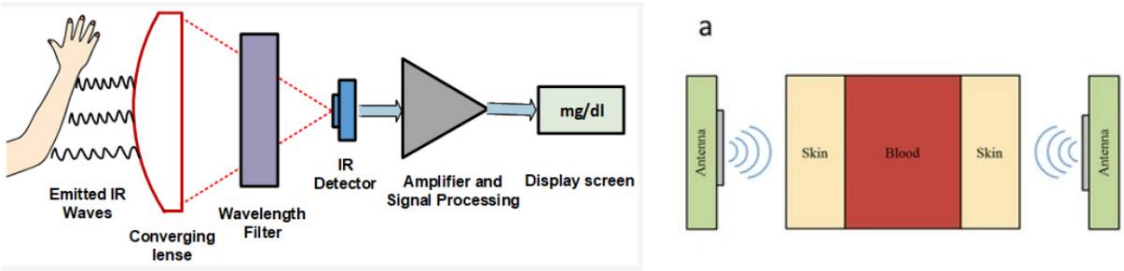

Figure1-3: Non-Invasive Blood Glucose Monitoring

Detecting low glucose concentrations in the blood poses a significant challenge for non-invasive methods due to the potential signal interference from various species and tissue components. Dominant interfering species include water content, proteins (albumin and hemoglobin), and fatty tissue. The concentration variations of these components among individuals further complicate accurate glucose concentration detection. Employing a glucose sensor with multiple wavelength sources offers a potential solution to this challenge. Each species exhibits a unique light attenuation coefficient dependent on the incident light's wavelength interacting with it.

The developed VIS-NIR optical sensor supports intensity measurements at multiple wavelengths, allowing for enhanced quantitative information extraction from light interactions with different species in aqueous glucose solutions. This study uses intensity data from 485nm, 645nm, 860nm, and 940nm light sources collectively to achieve higher sensitivity to glucose concentration changes.

The accuracy of glucose readings for any measurement device depends significantly on data analysis, particularly the intensity data, and associated glucose prediction models. Non-invasive glucose measurements' complexity necessitates more effective algorithms capable of handling higher-dimensional data to enhance accuracy. To predict glucose concentrations, various machine learning techniques like multiple linear regression, partial least square regression, principal component regression, feed-forward neural networks, deep neural networks, support vector machines, random forest regression, etc., are utilized. These regression-based models aim to minimize the error between actual and predicted glucose concentrations. However, they might have limitations in accurately predicting hyperglycemia and hypoglycemia, especially in real-life scenarios where multiple factors influence the measured signal.

According to the microwave sensing technique, the variations in glucose concentration cause the constitutive blood parameters (viz. dielectric constant and conductivity) to change. In other words, the blood glucose levels determine its dielectric constant and conductivity. Now, if a microwave resonator is loaded with different blood concentrations, its transmission and reflection coefficients will be affected.

Microwave sensors have been extensively reported by researchers to detect blood glucose levels at different frequencies. Dielectric resonator antennas, patch antennas, patch resonators, open-loop microstrip resonators, spiral microstrip resonators, split-ring resonators (SRRs), complementary electric-LC resonators (CELCRs), complementary

SRRs (CSRRs), and closed-loop resonators are also some examples of these sensors. The sensing approach here is significantly decided by the sensing parameter selected. Thus, different sensing parameters are often recruited to evaluate the sensitivity of microwave sensors, such as resonant frequency (fr) shifts, transmission (reflection) coefficient magnitude and phase, |S21| |S11|, and quality factor (Q factor). In some studies, sensor sensitivity is further extracted from a single measurement based on multiple sensing parameters.

For example, a range of configured SRRs, CELCRs, and CSRRs were utilized to measure resonant frequency (fr) and Δ|S| as sensing parameters for assessing blood plasma and glucose solutions.

Chapter2:

Infrared (IR) spectroscopy:

Infrared (IR) spectroscopy is one of the most common and widely used spectroscopic techniques. Absorbing groups in the infrared region absorb within a certain wavelength region. The absorption peaks within this region are usually sharper when compared with absorption peaks from the ultraviolet and visible regions. In this way, IR spectroscopy can be very sensitive to determination of functional groups within a sample since different functional group absorbs different particular frequency of IR radiation. Also, each molecule has a characteristic spectrum often referred to as the fingerprint. A molecule can be identified by comparing its absorption peak to a data bank of spectra. IR spectroscopy is very useful in the identification and structure analysis of a variety of substances, including both organic and inorganic compounds. It can also be used for both qualitative and quantitative analysis of complex mixtures of similar compounds.

The use of infrared spectroscopy began in the 1950's by Wilbur Kaye. He had designed a machine that tested the near-infrared spectrum and provided the theory to describe the results. Karl Norris started using IR Spectroscopy in the analytical world in the 1960's and as a result IR Spectroscopy became an accepted technique. There have been many advances in the field of IR Spec, the most notable was the application of Fourier Transformations to this technique thus creating an IR method that had higher resolution and a decrease in noise. The year this method became accepted in the field was in the late 1960's.

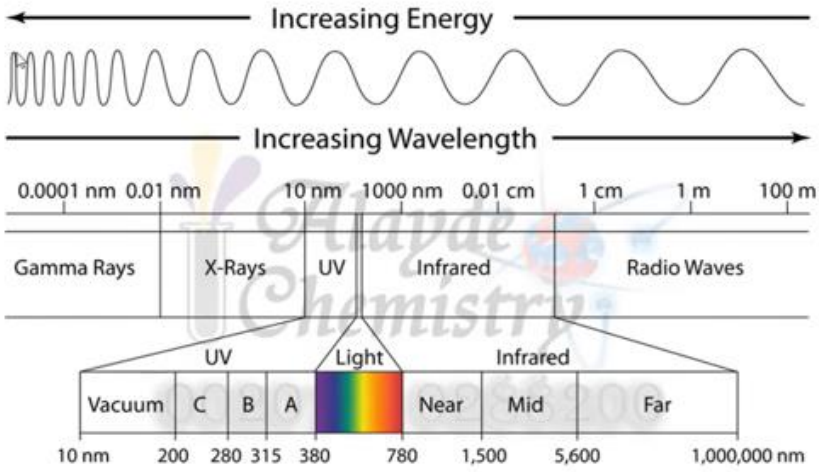

Figure2-1: The complete spectrum of electromagnetic radiation

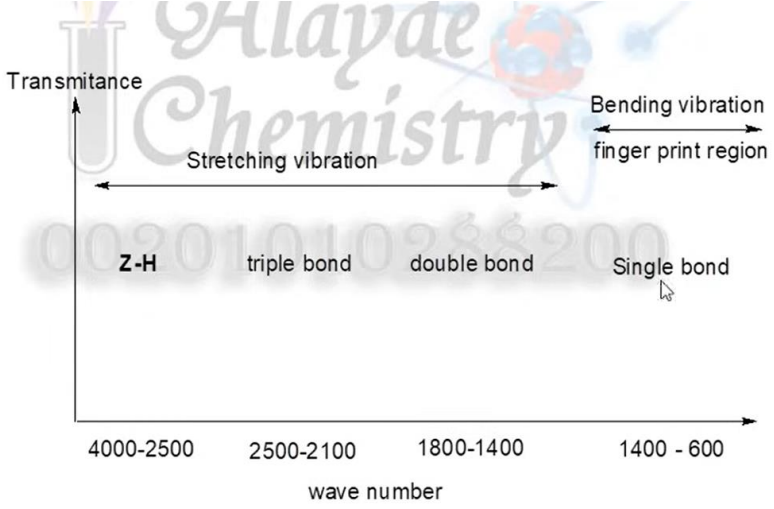

Figure2-2: the regions and characteristics of different vibrational modes in the infrared spectrum.

What are Infrared Waves?

Infrared waves, or infrared light, are part of the electromagnetic spectrum. People encounter Infrared waves every day; the human eye cannot see it, but humans can detect it as heat.

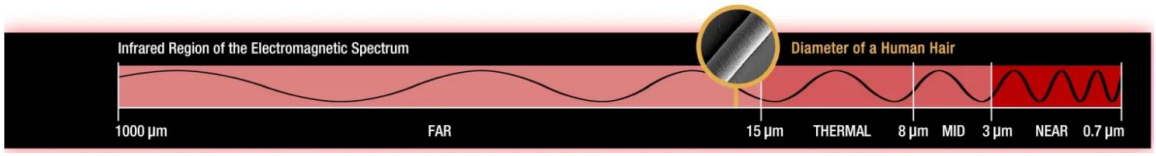

Figure2-3: infrared region of the electromagnetic spectrum.

Absorption Spectroscopy

There are three main processes by which a molecule can absorb radiation. and each of these routes involves an increase of energy that is proportional to the light absorbed. The first route occurs when absorption of radiation leads to a higher rotational energy level in a rotational transition. The second route is a vibrational transition which occurs on absorption of quantized energy. This leads to an increased vibrational energy level. The third route involves electrons of molecules being raised to a higher electron energy, which is the electronic transition.

It's important to state that the energy is quantized and absorption of radiation causes a molecule to move to a higher internal energy level. This is achieved by the alternating electric field of the radiation interacting with the molecule and causing a change in the movement of the molecule. There are multiple possibilities for the different possible energy levels for the various types of transitions.

The energy levels can be rated in the following order: electronic > vibrational > rotational. Each of these transitions differs by an order of magnitude. Rotational transitions occur at lower energies (longer wavelengths) and this energy is insufficient and cannot cause vibrational and electronic transitions but vibrational (near infra-red) and electronic transitions (ultraviolet region of the electromagnetic spectrum) require higher energies.

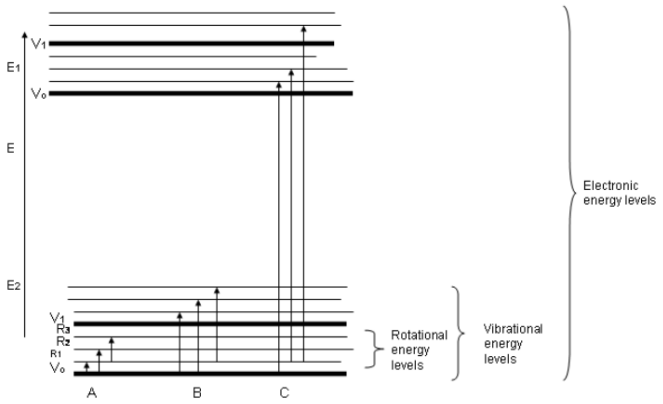

Figure 2-4: Energy levels for a molecule. Possible transitions that occur: (A): Pure rotational Transitions, (B) rotational-Vibrational Transitions, © Rotational-Vibrational Electronic Transitions

The energy of IR radiation is weaker than that of visible and ultraviolet radiation, and so the type of radiation produced is different. Absorption of IR radiation is typical of molecular species that have a small energy difference between the rotational and vibrational states. A criterion for IR absorption is a net change in dipole moment in a molecule as it vibrates or rotates. Using the molecule HBr as an example, the charge distribution between hydrogen and bromine is not evenly distributed since bromine is more electronegative than hydrogen and has a higher electron density.

HBr thus has a large dipole moment and is thus polar. The dipole moment is determined by the magnitude of the charge difference and the distance between the two centers of charge. As the molecule vibrates, there is a fluctuation in its dipole moment; this causes a field that interacts with the electric field associated with radiation. If there is a match in frequency of the radiation and the natural vibration of the molecule, absorption occurs and this alters the amplitude of the molecular vibration. This also occurs when the rotation of asymmetric molecules around their centers results in a dipole moment change, which permits interaction with the radiation field.

Molecules such as O2, N2, Br2, do not have a changing dipole moment (amplitude nor orientation) when they undergo rotational and vibrational motions, as a result, they cannot cannot absorb IR radiation.

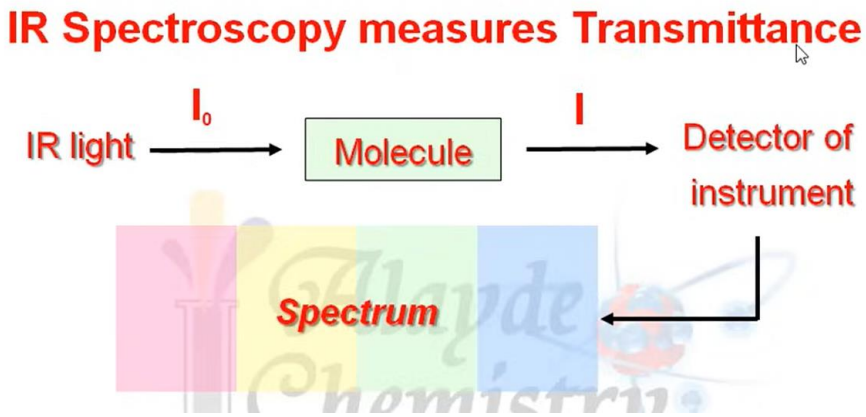

Figure 2-5:IR Spectroscopy measures transmittance

Region of IR

The IR region of the electromagnetic spectrum ranges in wavelength from 2 -15 μm. Conventionally the IR region is subdivided into three regions, near IR, mid IR and far IR. Most of the IR used originates from the mid IR region. IR deals with the interaction between a molecule and radiation from the electromagnetic region ranging (4000- 40 cm-1). The cm-1 is the wave number scale and it can also be defined as 1/wavelength in cm.

A linear wavenumber is often used due to its direct relationship with both frequency and energy. The frequency of the absorbed radiation causes the molecular vibrational frequency for the absorption process. The relationship is given below

$$\bar{v}(cm^{-1}) = \frac{1}{\lambda(\mu m)} \times 10^4 (\frac{\mu m}{cm}) = \frac{v(Hz)}{c(cm/s)}$$

Far InfraRed Spectroscopy: The far IR region is particularly useful for inorganic studies due to stretching and bending vibrations of bonds between the metal atoms and ligands. The frequencies, which these vibrations are observed, are usually lower than 650 cm-1. Pure rotational absorption of gases is observed in the far IR region when there is a permanent dipole moment present. Examples include H2O, O3, HCl.

Near InfraRed Spectroscopy: Absorption bands in the near infrared (NIR) region (750 - 2500 nm) are weak because they arise from vibrational overtones and combination bands. Combination bands occur when two molecular vibrations are excited simultaneously. The intensity of overtone bands reduces by one order of overtone for each successive overtone. When a molecule is excited from the ground vibrational state to a higher vibrational state and the vibrational quantum number v is greater than or equal to 2 then an overtone absorption results. The first overtone results from v = 0 to v = 2. The second overtone occurs when v =0 transitions to v = 3. Transitions arising from the near ir absorption are weak, hence they are referred to as forbidden transitions but these transitions are relevant when non-destructive measurements are required such as a solid sample. Near IR spectra though have low absorption they have a high signal to noise ratio owing to intense radiation sources and NIR is able to penetrate undiluted samples and use longer path lengths; it becomes very useful for rapid measurement of more representative samples.

Recent works in the literature show high accuracy in blood glucose prediction using NIR-based systems. They have been designed in reflectance and transmission modes. NIR spectroscopy, here, has been divided into two main subcategories: NIR spectrometry analysis and NIR PPG signal analysis. In NIR spectrometry analysis, logged voltage values after absorption and reflectance are measured, while in NIR PPG signal analysis, PPG signals are acquired using NIRLEDs.

Advantages of IR

High Scan Speed: Infrared spectroscopy can get information for the whole range of frequency simultaneously, within one second. Therefore, IR can be used to analyze a substance that is not very stable and finish the scan before it start to decompose.

High Resolution: The resolution of general prism spectrometer is only about 3 cm-1, but the resolution of infrared spectrometer is much higher. For example, the resolution of Grating infrared spectrometer could be 0.2 cm-1, the resolution of FT infrared spectrometer could be 0.1-0.005 cm-1.

High Sensitivity: With Fourier Transform, the infrared spectrometer doesn't need to use the slit and monochromator. In this way, the reflection specularity will be increased and the loss of energy in the analysis process will be decreased. Therefore the energy that reaches the detector is large enough and even very small amount of analytes could be detected. Nowadays, the infrared spectroscopy could detect the sample as small as 1-10 grams.

Wide Range of Application: Infrared spectroscopy could be used to analyze almost all organic compounds and some inorganic compounds. It has a wide range of application in both qualitative analysis and quantitative analysis. Also, the sample of Infrared spectroscopy doesn't have phase constraints. It could be gas, liquid or solid, which has enlarged the range of analytes a lot.

Large Amount of Information: Infrared Spectra could give us lots of structural information of the analytes, such as the type of compound, the functional group of compound, the stereoscopic structure of compound, the number and position of substituent group and so on. Depending on the available information form the functional part and the fingerprint part, infrared spectroscopy has become a great method to identify different kinds of compounds.

Non-Destructive: Infrared Spectroscopy is non-destructive to the sample.

Chapter3:

Measuring glucose with Near-Infrared (NIR) spectroscopy and how glucose interacts with Near-Infrared (NIR) spectroscopy:

Using the Near Infrared (NIR) Spectroscopy in glucose monitoring devices:

Near-Infrared spectroscopy is an optical method in which scattered, transmitted, or reflected light from the illuminated surface is studied. NIR waves lie in the EM bandwidth of 700–2500 nm. NIR spectroscopy finds its application in numerous fields like medicine, pharmaceutics, food analysis, quality control of chemical products, material sciences, astronomy, and agriculture. It has been investigated for glucose estimation for the last few decades. NIR waves have deeper penetration compared to MIR, so they can easily reach the dermis layer of skin and interact with blood components. Thus, NIR spectrometry can be utilized to estimate glucose levels in the blood. Another approach is to acquire PPG signals using NIR waves of specific

bandwidths for blood glucose estimation. PPG is an optical technique which detects volumetric changes in blood circulation. The PPG voltage signals are proportional to the quantity of blood flowing through the blood vessels. The changes in blood flow are seen as a waveform. The features obtained from these PPG signals are incorporated into machine learning algorithms to predict BGL. This technique has shown a better correlation with blood glucose.

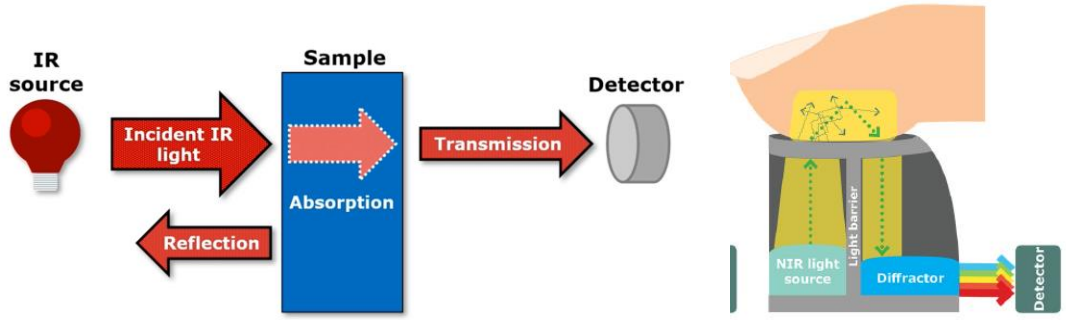

Figure3-1(a),(b): tissue molecules are affected by NIR light.

Effect of near infrared radiation (NIR) on tissue and blood:

Near-Infrared (NIR) spectroscopy is a vibrational spectroscopy technique, similar to Infrared and Raman spectroscopy. The interaction of molecules in the sample with electromagnetic waves stimulates the internal degrees of freedom (DOFs) of molecules, causing the bonds to vibrate at different frequencies based on their type and energy. This vibration pattern determines the spectral shape of the sample. NIR can be categorized into three regions based on bandwidth: the first overtone band (1400–2000 nm), the second overtone band (750–1400 nm), and the combinational band (2000–2500 nm).

NIR waves have maximum penetration depth in the skin compared to other infrared waves and are minimally absorbed by water and hemoglobin. Consequently, spectral measurements can be easily collected from the skin or body surface. Since Glucose is an example of a carbohydrate which is commonly known as blood sugar or dextrose. Its chemical formula is C6H12O6, and this empirical formula is shared by other structural sugars. So as NIR waves penetrate through skin tissue, they are partially scattered or absorbed. This phenomenon is related to the molecular vibrations of chemical bonds present in the medium and can be utilized to measure the concentration of biological functional groups such as C–H, N–H, C–O, and O–H in the blood.

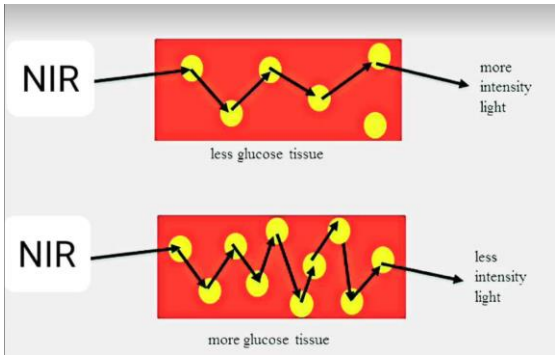

Figure3-2: Glucose molecules are affected by NIR light.

Detection of glucose molecule:

The reflectance and absorption of light using specific wavelength causes respective glucose molecular vibration which can be observed in glucose spectra (Yasuhiro and Ikehata 2016). The molecular vibrations exist in overall NIR region are called harmonics or overtones. Molecular vibration depends upon bond vibration like wagging, bending, rocking, stretching and twisting. It has been analyzed that multiple bonds stretch and wag at different resonant frequencies. It is also examined that absorption of light will depend on molecular concentration of the medium.

To determine informative bands for detection of glucose molecule, it is necessary to justify the resonant wavelengths of atomic bonds of blood glucose molecule. The structure of glucose molecule is shown in Fig.3-3. In long wave NIR region, the vibrations between OH and CH are represented which can be known as first overtone. Due to observations of molecular vibrations in short wavelength NIR region, it is analyzed that absorbance and reflectance are sharper and stronger in first overtone compared to second and third (higher overtones) overtones.

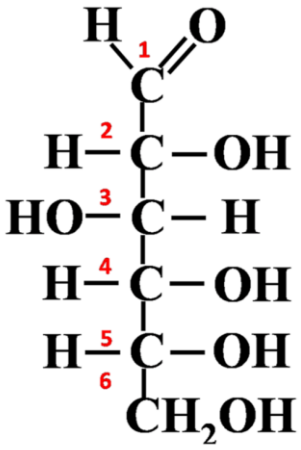

Figure3-3: Atomic structure of glucose molecule.

But the main drawback is that there is shallow penetration of the light in long wave NIR region (first overtone) in comparison with short wave NIR region. As per the given Fig. 3, a sharper and effective absorption has been elaborated in second overtone of the O–H bond inter-atomic vibration at 970 nm. This represents the presence of water molecule. At 840 nm, O–H bond of water is conflicted with C–H bond of fat. During absorption of light in presence of glucose molecule, vibration of C–H bond is examined near 910 nm. The vibration of CH2 is found near 930 nm. Glucose molecule detection is more precise using NIR long wave for in-vitro testing. NIR long wave will not give better results for in-vivo testing as long wave has shallow penetration. Opposite of this, short NIR wave has weak absorbance of glucose molecule but it has advantage of sharp penetration for in-vivo testing.

\also determined NIR informative wavebands for noninvasive blood glucose measurement. The glucose spectra in NIR region is represented in Fig.3-10. the NIR informative absorption peaks for glucose, water and lipid which as shown in figures 3-11, 12 and 13. explored the accuracy of non-invasive blood glucose measurement by short wavelength near infrared spectroscopy. These figures explain that CH vibration near 920 nm without overlapping of OH vibration of water molecule. elaborated near infrared spectra of sucrose, glucose and fructose. after analyzing CH2, CH and OH stretching in glucose molecule at 930 nm , 960 nm and 984 nm respectively.it was examined glucose apsorptions in short wave NIR region which is shown in Fig.3-4c.

After discussing these results, the 940 nm wavelength is proposed as one of the wavelengths for monitoring blood glucose levels in a non-invasive optical way to detect the glucose molecule.

According to literature of spectrum analysis of blood components, it is concluded that informative glucose absorption peaks exists in wave bands 920–960 nm and 1300–

1320 nm.Since the absorption of water and tissue at wavelengths (1300-1320 nm) is high, we suggest using LEDs with a wavelength of 940 nm. for blood glucose detection in proposed work.

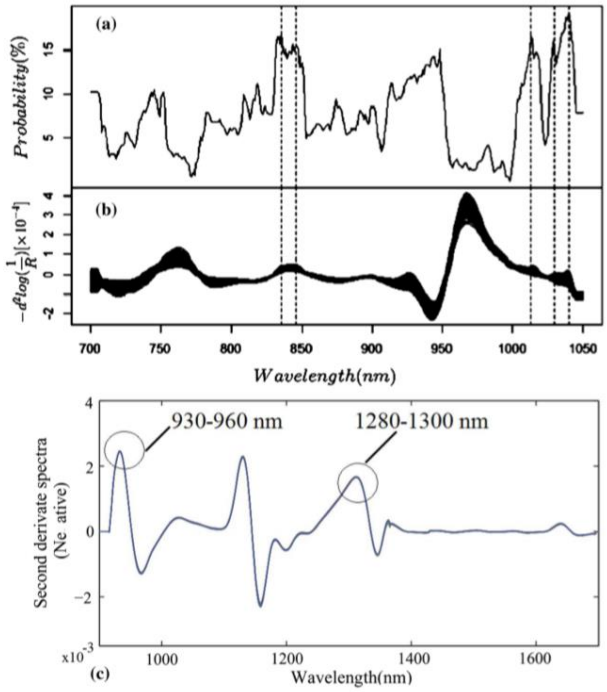

Figure. 3-4 a, b Glucose spectra in NIR region (700–1050 nm). c Glucose spectra in NIR region (900–1700 nm)

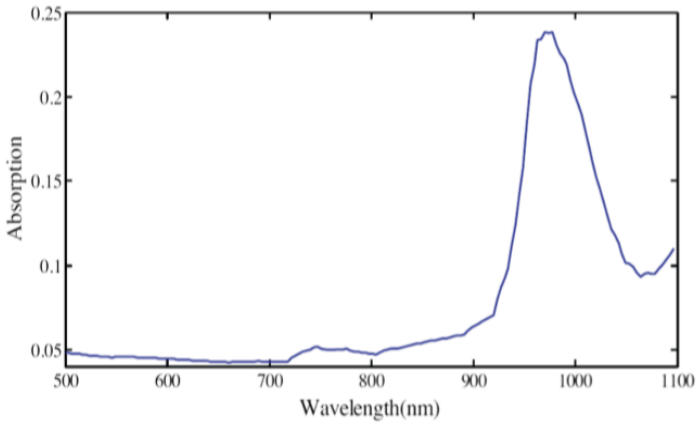

Figure3-5: Glucose spectra in NIR region

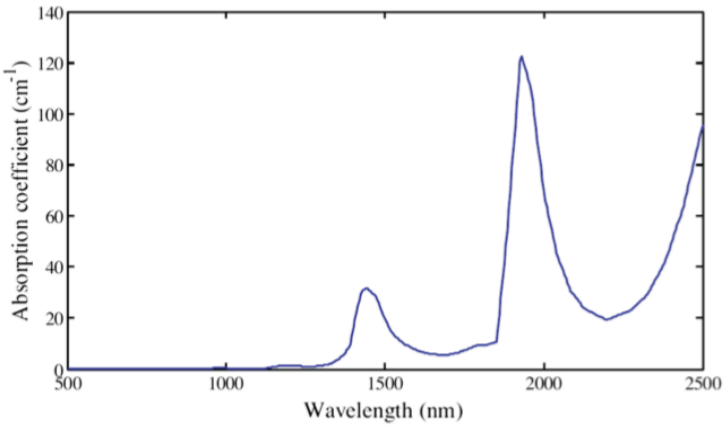

Figure3-6:Water spectra in NIR region

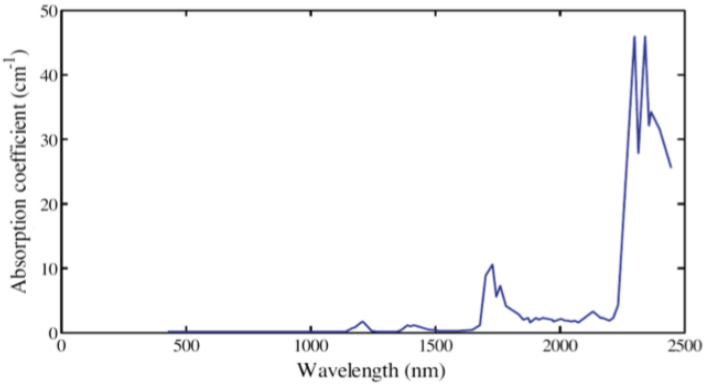

Figure3-7: Lipid spectra in NIR region

Selection of the NIR absorption wavelength:

according to the reference of the spectral region of the near-infrared wavelength As in the following figure. Glucose known to have more than one absorption point in NIR wavelength regions and these peaks can help to overcome the difficulty in determine the glucose reading.

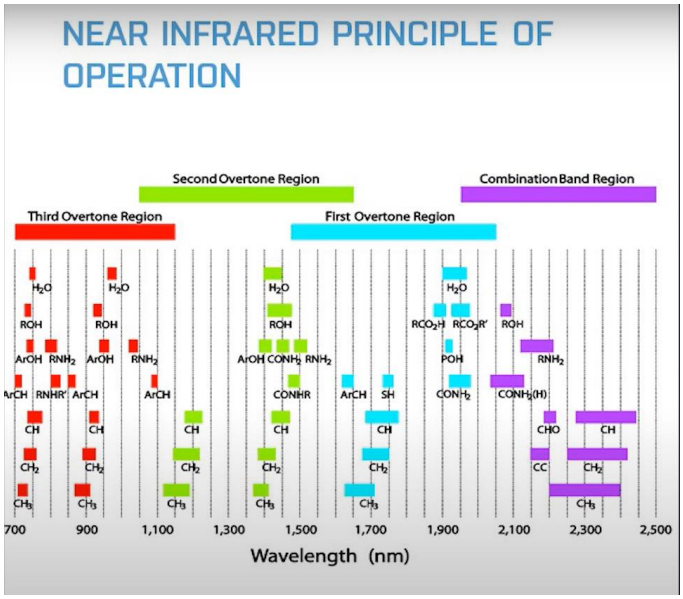

Figure3-8: The spectral region of the near-infrared wavelengths

Glucose molecules, which contain C–H and C–O bonds, exhibit absorption and reflectance of NIR waves passing through the skin. The NIR absorption for glucose isomers, such as fructose, lactose, and galactose, occurs at different wavelengths within the first overtones and combinational bands of NIR spectra. Importantly, these wavelengths do not coincide with the wavelength (940 nm) at which glucose absorption is being detected. Therefore, the presence of these isomers does not significantly affect the detection of glucose.

Absorption bands based on molecular composition

When a photon is incident on a molecule, there will be bond deformations or bond vibrations at different energy levels related to different bonds, depending on the energy of incident photon. So, only the photon with energy that corresponds to the difference between two of its energy levels can be absorbed. The frequency of the vibration is given by the

$$\vartheta = \frac{1}{2\pi}\sqrt{\frac{k}{m}} \qquad (1)$$

Where 'k' is the bond strength and 'm' is the reduced mass. For a glucose molecule, the molecular structure is as shown in the Figer bellow and the Table bellow shows the frequencies corresponding to different bond vibrations in glucose molecule.

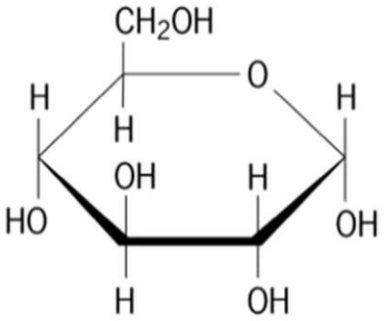

Figure3-9: Molecular structure of d-glucose

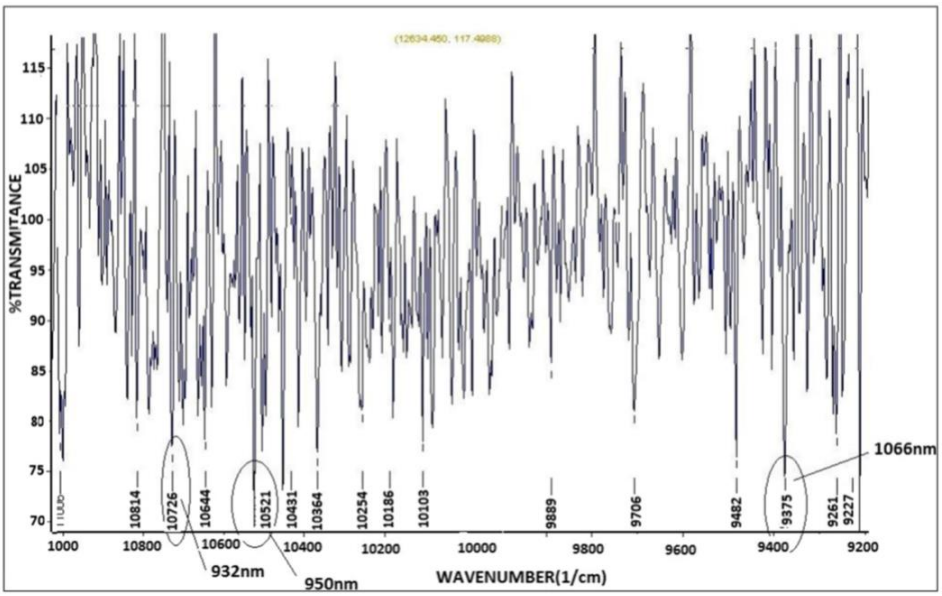

Figure3-9: Spectrum showing the transmittance of the glucose

Table3-1: Absorption band of glucose

Overtone	Wave length	bond	Wave length	bond
Fundamental	3377 nm	vC-H	2817 nm	vO-H
First overtone	1688 nm	2vC-H	1408 nm	2vO-H
Second overtone	1126 nm	3vC-H	939 nm	3vO-H

At a deeper level absorption of light can be seen as depen- dent on the probability of absorbance of a photon by the molecule. For nth overtone final energy is (n+1)*E, where E is the fundamental energy. As n increases, probability of absorbance decrease rapidly

and hence intensities of absorbance decrease as overtones increase. The absorption at fundamental frequency is calculated and from that the absorption at second overtone is calculated relativel. Table 2 depicts the relative absorptivity of C-H bond at different overtones with respect to the fundamental. It is evident that the absorptivity decreases rapidly as one goes from fundamental to the overtones in sequence.

Table:3-2 Relative absorptivity of C-H bond

Overtone	Wave number (cm^{-1})	Relative absorptivity
Fundamental	3019	1
First overtone	5912	0.088
Second overtone	8677	$3.2 * 10^{-3}$

Selection of sensor wavelength based on absorbance:

The absorption spectrum of the glucose has been studied in order to choose the wavelengths for LEDs. Figure 3-9 shows the absorption spectrum of the glucose over the second overtone region where the selected wavelengths are shown. We can observe that the absorption peaks in this region are very narrow typically of the order of the 2 to 5 nm but the LED emits the light over a range of wavelengths. The wavelengths are chosen such that the weighted average of the absorption over the spectral band- width of the LED is high. While calculating this weighted average the intensity of light emitted by the LED acts as weight for the absorption at that particular wavelength.

The expected value of the absorbance over a range has been calculated as:

$$E[A] = \int_{-\infty}^{+\infty} A(\lambda) * f(\lambda) d\lambda \qquad (2)$$

Where 'A' is the absorbance of glucose over a range of wavelengths and 'f(X)' is the probability density function of intensity of light emitted.

By multiplying the relative intensity of the light emitted by the LED shown in Fig. 3-10 and the absorbance value of glucose taken from the spectrum and averaging it over spectral distri- bution of LED we calculate the mean value of the absorbance which is shown in Fig. 3-11.

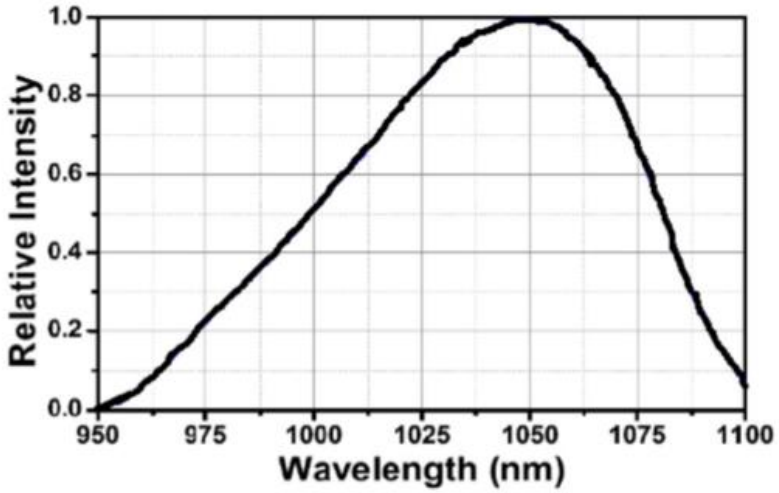

Figure3-10: Graph showing the relative sensitivity of light emitted by 1070nm LED

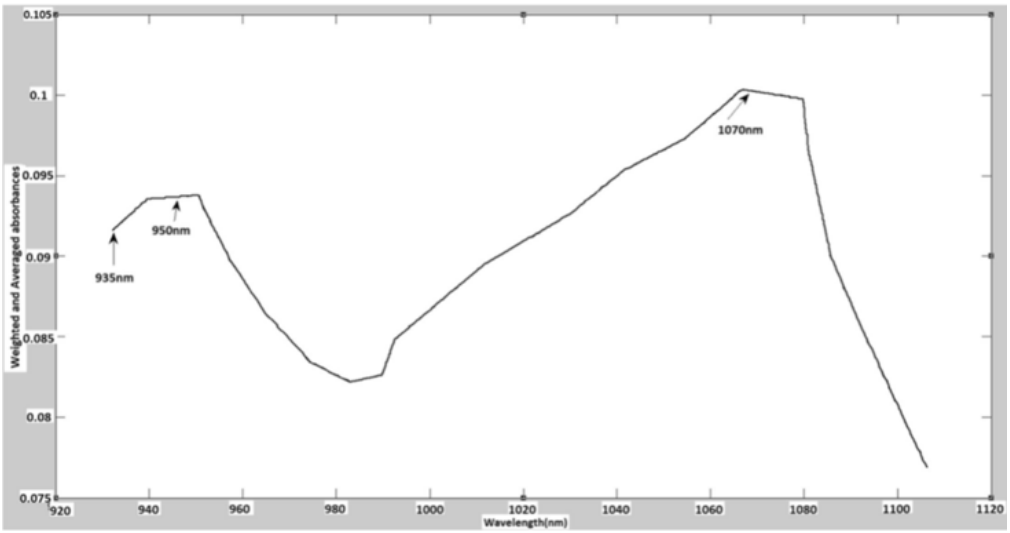

Figure3-11: Intensity weighted mean absorbance over 920 to 1100nm2

On the other hand, Numerous studies in the literature provide a detailed analysis of variations in NIR bandwidths and characteristic spectra due to changes in the concentration of glucose solutions. Both shorter regions of NIR (700-1300 nm) and longer regions (1300-1700 nm) have been investigated for glucose quantification. However, despite higher NIR bandwidths showing more prominent absorption by

glucose, they face challenges in penetrating finger tissues due to considerable scattering. As a result, long NIR wavelengths are unsuitable for the transmission method in noninvasive glucose measurements. Hence, current research is more focused on and emphasizes the study of short NIR regions for accurate glucose estimation in blood. The following section delves into recent studies on the application of NIR for blood glucose estimation.

Near-Infrared spectroscopy (NIRS) uses the light in the 750-2500 nm region, which interrogates the tissue with low-energy radiation. Radiation in the NIR range can penetrate the skin much deeper than visible or MIR radiation. The NIR spectral region has several windows where hemoglobin, lipid, and water absorption band intensities are low enough to allow light to penetrate into the tissue, enabling near-infrared spectral measurements. The specific absorption by compounds relevant to the diagnosis and monitoring allows safe and convenient in vivo measurement.

We can use LED with wavelength 940nm as a Transmitter and NIR Photodiode as a receiver. When a beam of Near-Infrared light us focused on a fingertip, it gets absorbed by glucose molecules present in the dermis layer. It is a medical fact that blood absorbs more light than its surrounding tissue. The concentration of glucose molecules will be higher in blood and therefore scattering of light by the glucose molecules will be higher in the case of a diabetic patient. Thereby, there will be more light coming out through the fingertip. Thus the reflected intensity will get increased in diabetic patients and vice versa for non-diabetic persons. this called NIR spectrometry analysis, In NIR spectrometry analysis, voltage values are logged after absorption and reflectance measurements.

NIR spectrometry analysis involves complex equations and algorithms, but a fundamental equation used in NIR spectrometry is the Beer-Lambert Law. This law relates the absorption of light to the properties of the material through which the light is traveling.

The Beer-Lambert Law is given by:

$$A = \varepsilon \cdot c \cdot l$$

Where:

A is the absorbance (no units, as it is a logarithmic ratio),

ε is the molar absorptivity or extinction coefficient (units: L mol−1−1cm−1),

c is the concentration of the compound in solution (units: mol L−1),

l is the path length of the light through the material (units: cm).

Chapter4:

Microwave Spectroscopy (MWS):

Microwaves range from 1 mm to 1 m in the EM wave spectrum. They are widely used in the fields of detection, communication, and medicine. As they can easily penetrate media with a millimeter of thickness, they can penetrate deep in skin tissue, reaching blood vessels in the dermis layer. The reflection, absorption, and transmission theory of microwaves through skin tissues can correlate to the changes in dielectric property, relative permittivity, and conductivity with fluctuating glucose concentrations. Hence, implying these waves can be used to estimate BGL.

Figure 4-1 shows the principle of MWS. The sensor is connected to a vector network analyzer (VNA) which detects changes in amplitude and phase corresponding to changes in permittivity of the sample, as shown in Figure 4-1. MWS is sensitive to a small glucose concentration; it can be easily designed and is low cost. Unfortunately, it has poor selectivity, as blood components affect the measurement parameters such as the dielectric constant. MWS is also sensitive to physiological parameters like breathing, sweating, and physical activities.

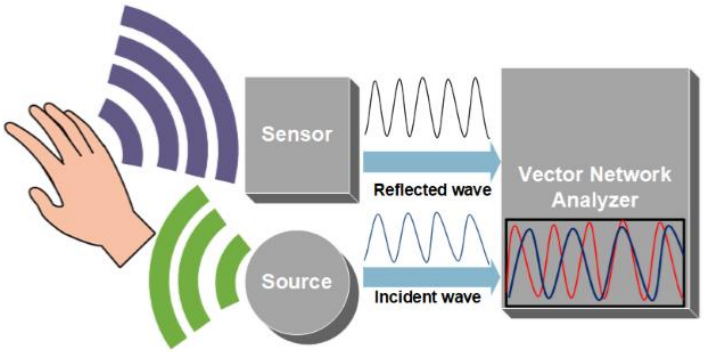

Figure 4-1: Microwave Spectroscopy working principle.

RF and Microwave Sensors:

The field of radio frequency (RF) and microwave engineering generally covers the behavior of alternating current signals with frequencies in the range of 1 MHz (1 MHz = 10^6 Hz) to 1000 GHz (1 GHz = 10^9 Hz).

The term microwave is typically used for frequencies between 300 MHz and 300 GHz (as illustrated in Fig.4-2), with a corresponding electrical wavelength between $\lambda = c/f = 1m$ and $\lambda = 1$ mm, respectively.

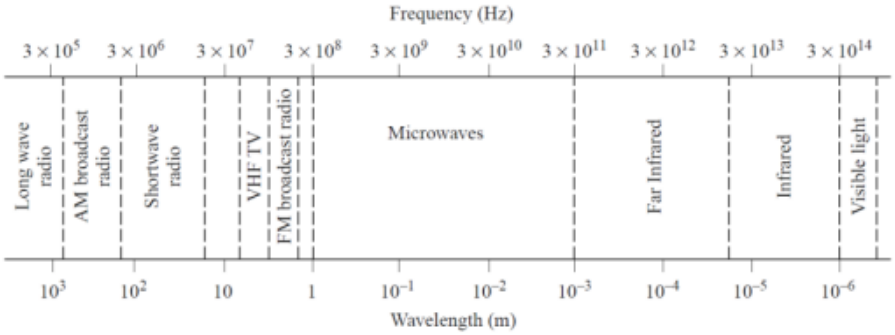

Figure4-2: the range of microwave wave length:

Microwave frequency range:

Microwave sensors work at the microwave frequency and generate or respond to an electromagnetic field. Due to their small size, low cost, and ease of fabrication, microstrip resonators have become popular for measuring material characterization.

Scattering parameters are often used to describe how RF energy spreads through multi-port networks, allowing us to view a complex network as a "black box." In the context of two-port networks, as illustrated in Fig. 4-3, these parameters provide valuable insights into the behavior of the system.

In a multi-port network, when an RF signal is incident on one port, several outcomes can occur. A fraction of the signal may get reflected back out of the incident port, represented as $V1-$ for port 1, while some of it enters the incident port and then scatters to some or all of the other ports, potentially undergoing amplification or attenuation. Additionally, a portion of the incident power may convert to heat or electromagnetic radiation.

To clarify, $V1+$ represents the incident voltage at port 1, while $V1-$ corresponds to the reflected voltage at port 1. Similarly, $V2+$ and $V2-$ denote the incident voltage and reflected voltage at port 2, respectively. This description outlines the fundamental concept of scattering parameters in the context of two-port networks.

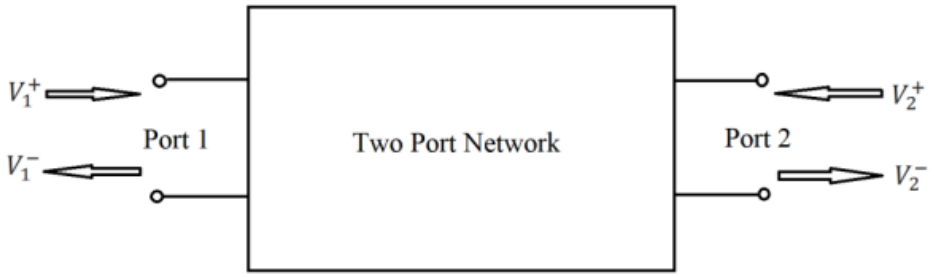

Figure4-3: Diagram of a two port network

If we define the normalized voltage waves as $a1$, $b1$, $a2$, $b2$ as shown in Fig. 4-4 and describe the characteristic impedance of port 1, $Z01$, and the characteristic impedance of port 2, $Z02$, the normalized voltage waves would be defined as follows:

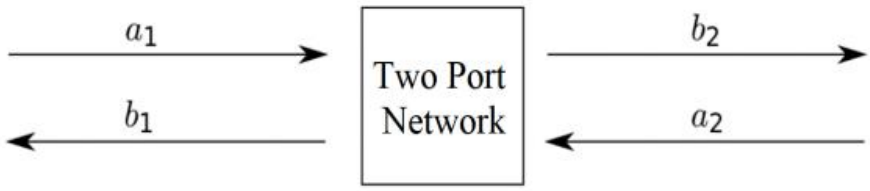

Figure 4-4: Normalized voltage waves in a two port network

$$a_1 = \frac{V_1^+}{\sqrt{Z_{01}}}, \qquad b_1 = \frac{V_1^-}{\sqrt{Z_{01}}},$$
$$a_2 = \frac{V_2^+}{\sqrt{Z_{02}}}, \qquad b_2 = \frac{V_2^-}{\sqrt{Z_{02}}}. \qquad (1.1)$$

Based on the definition of scattering parameters, they can be described as follows based on normalized voltage waves.

$$S_{11} = \frac{b_1}{a_1}, \qquad S_{12} = \frac{b_1}{a_2},$$
$$S_{21} = \frac{b_2}{a_1}, \qquad S_{22} = \frac{b_2}{a_2}. \tag{1.2}$$

If the characteristic impedance of both ports are equal, then the scattering parameters are as in Eq. (1.3) based on incident and reflected waves.

$$S_{11} = \frac{V_1^-}{V_1^+}, \qquad S_{12} = \frac{V_1^-}{V_2^+},$$
$$S_{21} = \frac{V_2^-}{V_1^+}, \qquad S_{22} = \frac{V_2^-}{V_2^+}. \tag{1.3}$$

The S-parameters have the following generic descriptions:

*S*11 is the input port voltage reflection coefficient

*S*12 is the reverse voltage gain

*S*21 is the forward voltage gain

*S*22 is the output port voltage reflection coefficient.

In this project, one-port and two-port networks are examined. The one-port microwave resonator (patch antenna) focuses on the *S*11 parameter, as it constitutes a single-port network. For the two-port microwave resonators (ring resonator and CCSR), *S*11 and *S*21 are the primary parameters of interest. It's noteworthy that *S*22 and *S*12 are equivalent to *S*11 and *S*21 due to the design's symmetry.

Measuring glucose with microwave resonators and how glucose interacts with and microwave resonators:

To differentiate blood samples with various glucose levels based on their permittivity, it is crucial to choose a frequency for the sensor designs that shows sensitivity to the permittivity change. Previous studies have shown a correlation between glucose levels and blood's permittivity.

The complex permittivity of a material is given by:

$$\varepsilon = \varepsilon' - j\varepsilon''$$

where ε' is the dielectric constant or the relative permittivity and " quantifies the material's loss and can be defined as:

$$\varepsilon'' = \sigma/\omega\varepsilon_0$$

Where σ is the conductivity of the material, ω is the angular frequency, and ε_0 is the permittivity of free space (8.85×10^{-12} F/m).

As shown in Fig. 4-5, four dispersion regions of an ideal biological tissue are described as α, β, δ, and γ in [7]. The imaginary part of the dielectric constant of a biological tissue does not change significantly over different frequencies. In contrast, a substantial change in the real part with frequency alteration is seen, and that is what will be taken advantage of in this project.

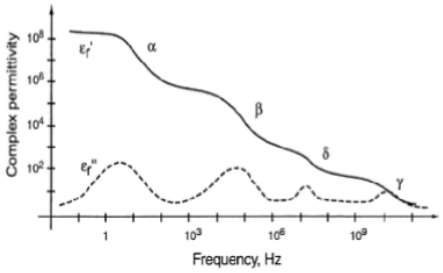

Figure4-5: Dispersion (region of decreasing dielectric constant) regions of ideal biological tissues.

The permittivity of the biological tissues is often represented by the "Cole-cole" model with the following equation:

$$\varepsilon(\omega) = \varepsilon'(\omega) - j\varepsilon''(\omega)$$
$$= \varepsilon_\infty + \sum_n \frac{\Delta\varepsilon_n}{1 + (j\omega\tau_n)^{(1-a_n)}} + \frac{\sigma_i}{j\omega\varepsilon_0}$$

where (ω) is the complex permittivity of the specific tissue, τn is time constant, ∞ is the permittivity at high frequencies, and a is distribution parameter used to measure broadening of the dispersion region.

As shown in Fig. 4-6, blood permittivity is constant for frequencies less than 1 MHz. According to Fig. 4-5, it can be concluded that the δ dispersion region is a potentially effective region to study the relative dielectric constant changes. The δ dispersion region is in the microwave frequency range and all of the designs in this project operate in this range.

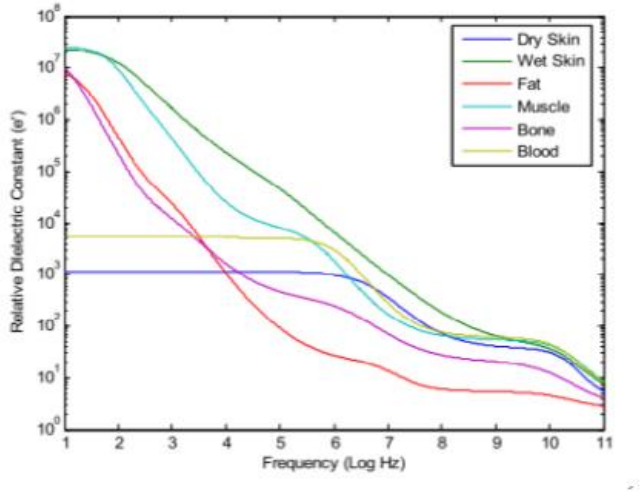

Figure4-6: Relative dielectric constant of different tissue layers in a frequency range of 10 Hz to 100 GHz

The resonant frequency of the designs was chosen to be between (2.4-3) GHz. This frequency is approved by Food and Drug Administration (FDA) and it is also used in Wi-Fi devices. A non-invasive blood glucose monitoring system would consist of digital parts for data processing and an RF/microwave circuit board that functions similar to a vector network analyzer (VNA) and we will use NanoVNA V2 3G module.

A review on previous works for microwave sensor design for a noninvasive glucometer includes design analysis, sensor configurations, and simulation results of the designs with no materials applied to the resonators. The investment in the development of a human tissue model with five different types is discussed, along with the placement of the tissue models on the sensors. A comparison between sensors based on their responses is also provided in this project, culminating in the final conclusion on the performance of the sensors and their efficiency.

The correlation between permittivity and glucose concentration has been studied in several countries. For instance, authors fed a hamster glucose in water and measured its tail dielectric constant to demonstrate this correlation. The permittivity obtained from the Cole-cole equation was compared to a microwave resonator's response to illustrate this correlation. Monitoring using microwave resonators is presented.

Patch Resonator: A patch resonator, as shown in Fig.4-7, was proposed, with its resonant frequency at 2.45 GHz when radiating towards the tissue. CST Microwave Studio software was used for the simulation. The resonator is fed from the back of two feeding ports using SMA connectors.

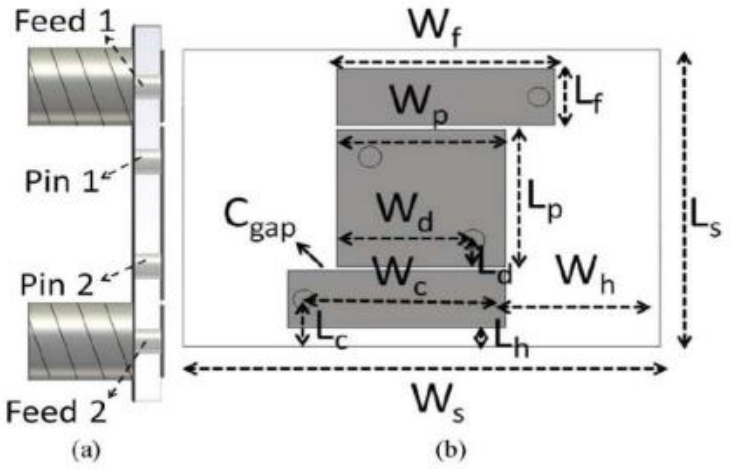

Figure4-7: Patch resonator: (a) side view; (b) top view

Input impedance was studied using the Z-parameter response of the resonator calculated where the load impedance (ZL) was considered matched to 50 Ohms.

$$Z_{in} = Z_{11} - \frac{Z_{12}Z_{21}}{Z_{22} + Z_L}$$

Interaction of S11 and S21 with Permittivity:

Understanding S11and S21:

S11: This represents the reflection coefficient. It measures how much of the electromagnetic wave is reflected back from the microstrip resonator. A high S11 value indicates more reflection, and a low S11 value indicates less reflection.

S21: This represents the transmission coefficient. It measures how much of the electromagnetic wave passes through the microstrip resonator. A high S21 value indicates more transmission, and a low S21 value indicates less transmission.

Interaction with Permittivity:

Permittivity (ε): This is a measure of how much resistance is encountered when forming an electric field within a medium. The permittivity of a medium changes with the presence of different substances, such as varying glucose levels in blood.

How Permittivity Affects S11 and S21:

Change in Resonant Frequency

The resonant frequency of a microstrip resonator is highly sensitive to changes in the permittivity of the surrounding medium.

When the permittivity changes (e.g., due to varying glucose concentration in blood), the resonant frequency of the microstrip resonator shifts.

This shift can be detected by observing changes in S11 and S21 parameters.

S11 - Reflection Coefficient:

Higher Permittivity: If the permittivity of the medium increases, the resonant frequency of the resonator might decrease. This results in a change in the impedance matching conditions, causing a variation in the reflection coefficient S11. The dip in S11 indicates a frequency where the impedance match is optimal.

Lower Permittivity: If the permittivity decreases, the resonant frequency might increase. This again affects the reflection coefficient, resulting in a different value of S11 at resonance.

S21 - Transmission Coefficient:

Higher Permittivity: An increase in permittivity affects the transmission path of the wave through the resonator. At the new resonant frequency, S21 might show a peak or dip depending on how well the wave propagates through the resonator.

Lower Permittivity: A decrease in permittivity will also shift the transmission characteristics, altering the S21 value at the new resonant frequency.

Practical Implications:

Measurement:

By measuring the changes in S11 and S21, one can infer the changes in the permittivity of the medium.

For glucose monitoring, as the glucose concentration changes, it alters the blood's permittivity, thereby shifting the resonant frequency of the microstrip resonator.

Calibration:

Calibrate the microstrip resonator with known glucose concentrations to create a reference curve of S11 and S21 values versus glucose levels.

Use this reference during actual measurements to determine unknown glucose concentrations based on observed S11 and S21 values.

Summary:

S11 measures the reflected wave and is affected by the impedance match, which is sensitive to changes in permittivity.

S21 measures the transmitted wave and is also influenced by the medium's permittivity.

By monitoring the shifts in resonant frequency and the corresponding changes in S11 and S21, one can deduce changes in the medium's permittivity, which in the context of the project, correlates to blood glucose concentration.

Microwave Resonator Design:

1. Microstrip Patch Antenna:

A microstrip patch antenna consists of a rectangular metal trace on top of a dielectric substrate with a ground plane underneath. As shown in Fig. 4-8, there is only one port and as a result, $S11$ is the only scattering parameter. Patch antennas can be fed by various techniques

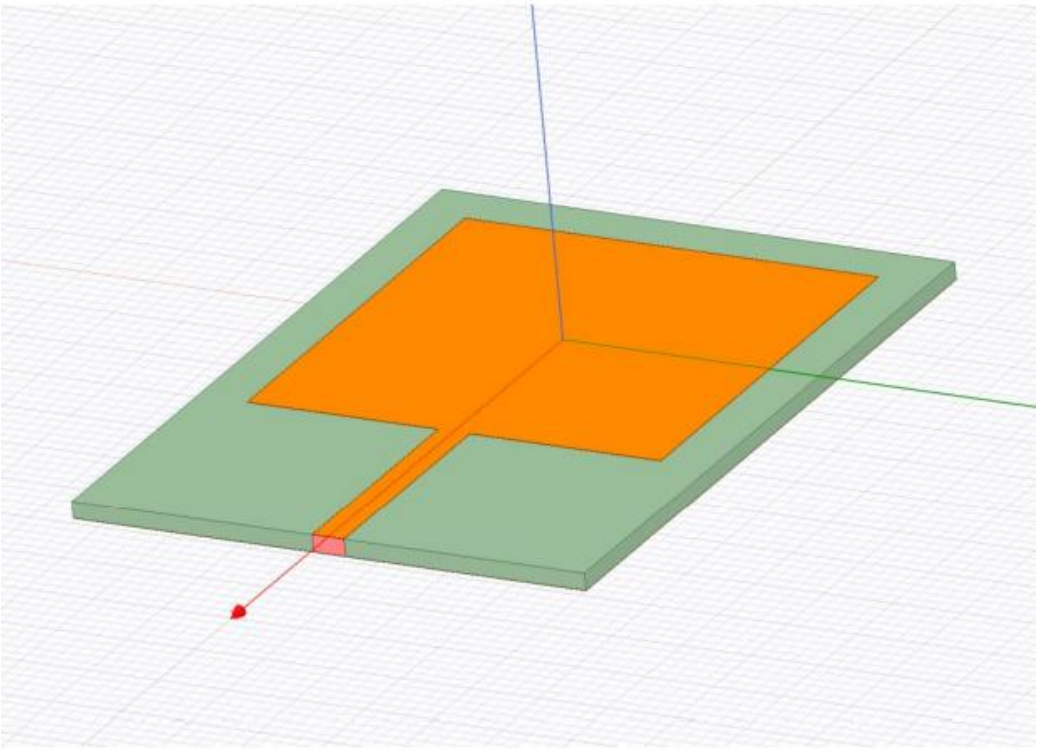

Figure4-8: Patch antenna model in ANSYS HFSS using a microstrip line as a feed line

The width and length of the rectangle patch antenna is derived using equations:

1) $$W = \frac{c}{2f_r} \times \sqrt{\frac{2}{\varepsilon_r+1}}$$

2) $$\Delta L = 0.412h \times \frac{(\varepsilon_{eff}+0.3)}{(\varepsilon_{eff}-0.258)} \times \frac{(\frac{W}{h}+0.264)}{(\frac{W}{h}+0.8)}$$

$$L = \frac{1}{2cf_r\sqrt{\varepsilon_{eff}}} - 2\Delta L$$

3)

where W is the width of the patch antenna, L is its length, h is the height of the substrate, c is speed of the light $(3 \times 10^8\ {}^{m}/_{s})$. ε_r is the relativetivity of the substrate, and εeff is the effective permittivity and can be obtained

The width, length and height of the substrate should satisfy the following conditions:

$$L_{substrate} = L + 6h$$

$$W_{substrate} = W + 6h$$

$$h \geq 0.06\frac{\lambda_{air}}{\sqrt{\varepsilon_r}}$$

The width of the microstrip line (feed line) was calculated at 2.29 mm at a 2.4 GHz resonant frequency to match the 50 Ω characteristic impedance using Eq. (3.7) and Eq. (3.8). The length of the transmission line were designed at one quarter of a wavelength which was calculated using Eq. (3.9). For 2.4 GHz, a quarter wavelength is calculated to be 17.1243 mm.

$$\varepsilon_{eff} = \begin{cases} \frac{\varepsilon_r+1}{2} - \frac{\varepsilon_r-1}{2}\left[\frac{1}{\sqrt{1+12\left(h/w\right)}}\right] & for\ {}^{w}/_{h} \geq 1 \\ \frac{\varepsilon_r+1}{2} - \frac{\varepsilon_r-1}{2}\left[\frac{1}{\sqrt{1+12\left(h/w\right)}} + 0.04\left(1-\left({}^{w}/_{h}\right)^2\right)\right] & for\ {}^{w}/_{h} < 1 \end{cases} \quad (3.7)$$

$$Z_0 = \begin{cases} \frac{120\pi}{\sqrt{\varepsilon_{eff}}\left[{}^{w}/_{h} + 1.393 + {}^{2}/_{3}\ln\left({}^{w}/_{h} + 1.444\right)\right]}\ (\Omega) & for\ {}^{w}/_{h} \geq 1 \\ \frac{60}{\sqrt{\varepsilon_{eff}}}\ln\left(8\,{}^{h}/_{w} + 0.25\,{}^{w}/_{h}\right)(\Omega) & for\ {}^{w}/_{h} < 1 \end{cases} \quad (3.8)$$

$$\lambda = \frac{c}{f\sqrt{\varepsilon_{eff}}} \quad (3.9)$$

where $Z0$ is the characteristic impedance (50 Ω), h is the height of the substrate, w is the width of the transmission line, and the λ is the wavelength. To improve impedance matching and sharpen the resonance response, two inset cuts in the patch where it meets the feed line were used as shown in Fig 4-9. The dimensions of the set cut is By changing

these dimensions the impedance of the line can be closely matched to the characteristic impedance.

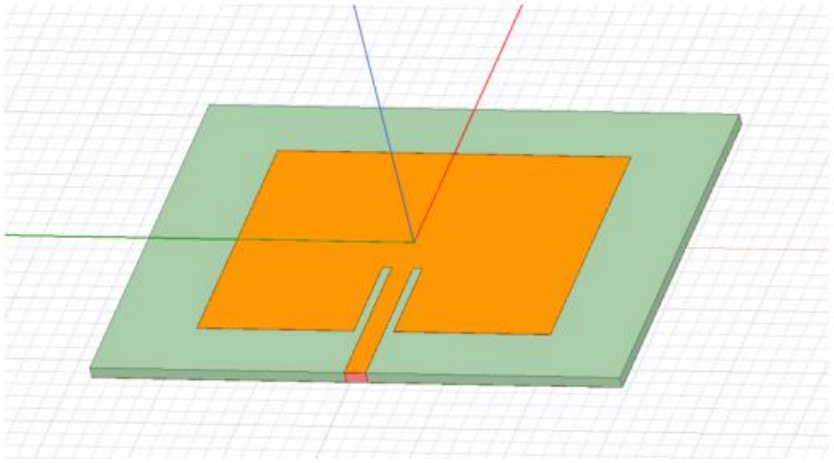

Figure4-9. Patch antenna model in ANSYS HFSS using inset cut feed.

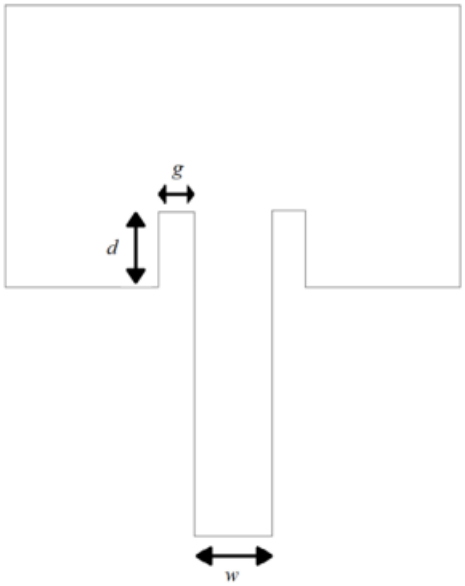

Figure4-10: Inset cut dimensions; (d as the length of the inset cut and g is its width) and the width of the microstrip line (w) illustrated on a patch diagram.

Since w/20 was offered as the best value for the inset cut's width (g) in, 1.9 mm was chosen for g. The inset cut's length (d) was obtained from Eq. (3.10) as 10.355 mm

$$d = \frac{L}{\pi}\cos^{-1}\left(\sqrt{\frac{Z_0}{Z_{in}}}\right)$$

where Zin is the input impedance of the patch which was calculated using Eq. (3.11), L is the length of the patch, and $Z0$ is the characteristic impedance (50 Ohms)

$$Z_{in} = 90\left(\frac{\varepsilon_r^2}{\varepsilon_r - 1}\right)\left(\frac{L^2}{W^2}\right)$$

2. CSRR-based sensor desine:

The proposed sensor design incorporates four cells of hexagonal-shaped complementary split ring resonators (CSRRs):

The sensor architecture incorporates four hexagonal-shaped **complementary split-ring resonators** (CSRRs) arranged in a honey-cell configuration on a thin FR4 dielectric substrate. These CSRR sensing elements are interconnected via a planar microstrip-line to a radar board operating within the ISM band of 2.4–2.5GHz.

The integrated sensor showcases remarkable detection capability and sensitivity to blood glucose levels. This performance is credited to the optimized design of the CSRR sensing elements, which expose glucose samples to intense electromagnetic fields concentrated around the sensing region during resonant states. This unique feature enables the sensor to discern subtle variations in electromagnetic properties associated with differing glucose levels.

Validation of the sensor's functionality is carried out through in-vitro measurements using a Vector Network Analyzer (VNA), revealing significant frequency-shift responses when the sensor interacts with glucose samples ranging from 70 to 120 mg/dL.

CSRR-based sensor design:

The proposed biosensor is numerically designed to operate around 2.45 GHz when used for glucose detection. This frequency is chosen to match the Industrial, Scientific, and Medical (ISM) band 2.4–2.5 GHz when the sensor is integrated with the radar system. In fact, operating in this frequency range would also allow adequate penetration depth for the induced EM waves to reach the blood vessels in the fingertip. This penetration is maximized to a certain extent in our sensor given the concentrated energy of the sensing

region where the fingertip is placed. Additionally, at this frequency, there is a higher possibility to identify different glucose concentrations of interest due to the small loss introduced.

Therefore, sensing at this frequency would probably bring considerable sensitivity despite the small changes in dielectric properties from one glucose level to another. A slight increase in $\varepsilon r'$ and, conversely, a tenuous decrease in $\tan\delta$ are observed with an increased glucose concentration. In this tendency, it is also observed that the percent variation in $\tan\delta$ is much higher than its corresponding in $\varepsilon r'$ (e.g., for a 10 mg/dL change at 2.4 GHz, the percent change in $\tan\delta$ is about 0.4%, while the variance in $\varepsilon r'$ is approximately 0.005%).

The sensor structure is primarily inspired by metamaterial technology, incorporating four similar cells of hexagonal-shaped complementary split-ring resonators (CSRRs) with localized elements in a novel configuration. The four CSRRs are configured in a honey-cell pattern and engraved at a depth of 35 µm in the copper ground plane of an FR4 dielectric PCB. The dielectric permittivity of the substrate is $\varepsilon r' = 4.4$, with a loss tangent $\tan\delta = 0.02$. The dimensions of the PCB are length L = 66 mm, width W = 20 mm, and thickness h = 0.8 mm. The magnetic walls of the passive CSRRs are oriented perpendicularly to a planar microstrip-line (MTL) etched on the upper face of the substrate. The dimensions of the feed line are optimized to 66 × 1.5 mm^2 to obtain a 50 Ω characteristic impedance matching the SMA (SubMiniature version A (fig. a)) connectors of the driving power source.

Two topologies for the honey-cell configuration are realized: compact and dispersed. In the compact configuration, two hexagonal cells are placed horizontally along the axis of the MTL strip with a distance of CL = 12.6mm between their corresponding geometric centers. Additionally, two hexagonal cells are placed vertically with a distance of CW = 12 mm between their corresponding centers. Each CSRR unit-cell is composed of two concentric rings (outer and inner) of hexagonal shape nested within each other, with a coupling gap of t = 0.4 mm in between. The loop of each ring has a dielectric slit of side-width s = 0.4 mm and ends in a metallic slot of width g = 0.4 mm. The diagonal length of the outer ring is a = 7.6 mm, while that of the inner one is set to b = 6.0 mm. The split gaps for both rings are on diametrically opposite sides of each other.

Figure4-11:SMA Connectors

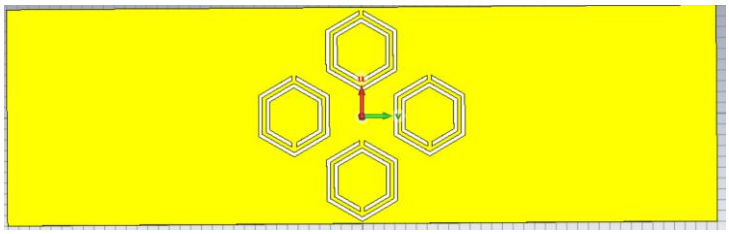

Figure4-12(a): configuration of the CSRRs sensing elements in the ground copper plane (top view).

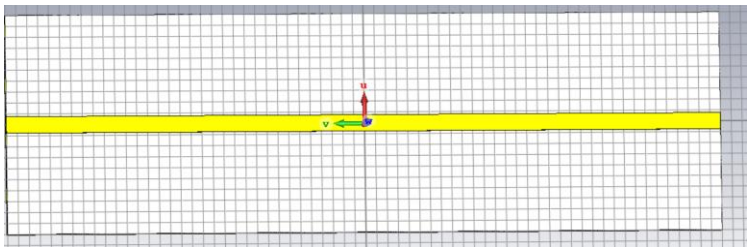

Figure4-12(b): CCSRs model in CST.

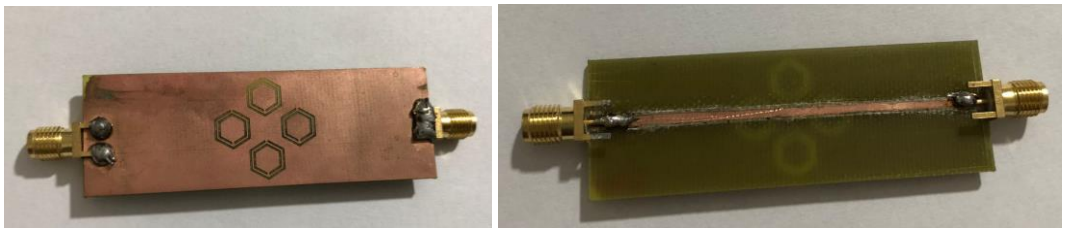

Figure4-12(c):The fabricated of CCSRs

3. Design of 1-CSRR Sensor:

The sensor is fabricated on a DiClad880 substrate (εr = 2.2, tan δ = 0.0009) with a thickness of 1.6 mm. The dimensions of the sensor structures are as follows: W1 = 40 mm, W2 = 20 mm, W3 = 0.8 mm, W4 = 1.2 mm, W5 = 5 mm, L1 = 45 mm, L2 = 30 mm, L3 = 7.3 mm,L4 =9.6 mm, L5 = 9.25 mm, S = 0.6, R = 6.4 mm, C = 0.6 mm, G = 0.4 mm, and θ = 60◦ The input of the sensor is attached to an SMA connector for microwave excitation and measurement. A printed circuit board (PCB) method was used to fabricate the sensor at room temperature in a research unit laboratory, which is a low-cost and simple process, as shown in Figure below.

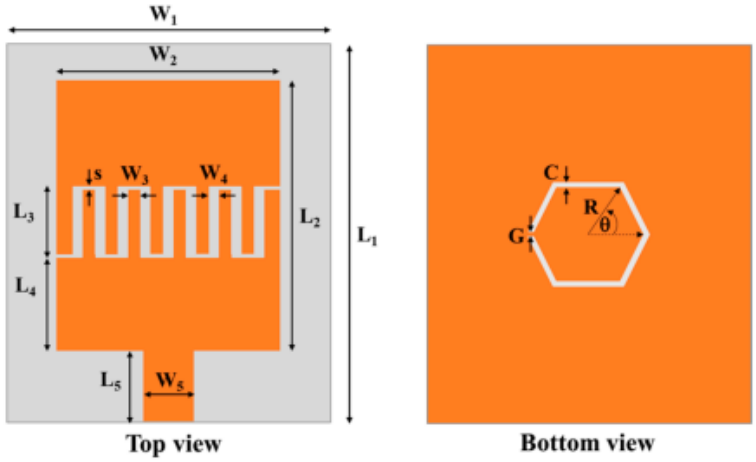

Figure4-13(a),(b):

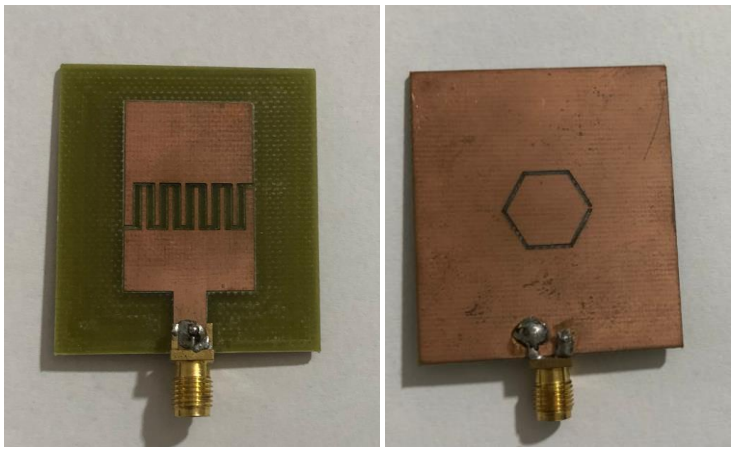

Figure4-14:The fabricated hexagonal CARR microwave sensor is shown in figure below the top view.

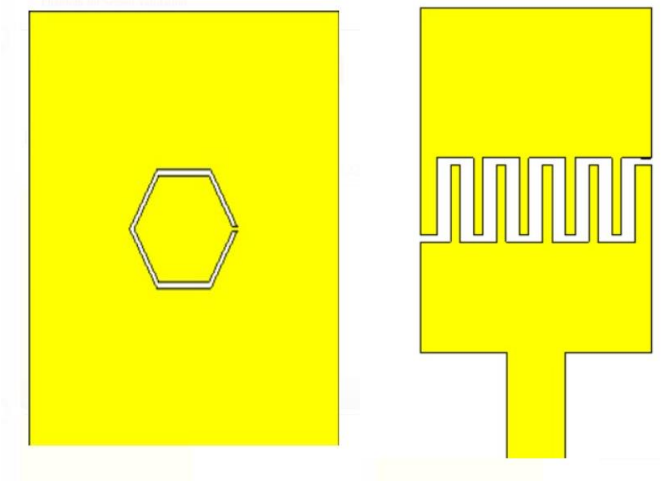

Fig:(a) fig : (b)

Figure4-15: (a) and (b): 1-CSRR Sensors model in CST.

4. Design Stepped Impedance Resonator Sensor:

Microwave sensing using small, printed high-frequency sensors is one of the promising techniques to implement non-invasive glucose monitoring The general principle is to utilize electromagnetic waves to characterize the material under test (MUT), based on its dielectric properties and measuring its resonant frequencies. Previous studies have found that these resonant frequencies correlate to dielectric permittivity of the material and shift with varying concentrations of glucose Permittivity values are inversely proportional to glucose concentration, where higher concentrations result in lower permittivity values. Different designs of radio frequency Of which:

Stepped Impedance Resonator Sensor The sensors were fabricated on a Flame-Retardant 4 (FR4) substrate, a common substrate for printed circuits. The FR4 printed circuit board has a thickness of 1.57 mm, with relative permittivity of 4.7, and loss tangent of 0.014 An important parameter that affects the sensitivity of the sensor is its Quality (Q) factor. The Q factor describes the relation between stored energy and energy usage rate and is used to describe the efficiency of the device. The basic Q-factor equation is dependent on the energy loss of the components in the device such as inductor, capacitor, or resistor. Q can also be calculated using the following equation from the S11 frequency response

$$Q = \frac{f}{\Delta f_{3dB}} = 2\pi \frac{Energy\ stored}{Energy\ loss} = \frac{1}{R}\sqrt{\frac{L}{C}}$$

The highest value obtained for the Q factor was at the dimensions in which we designed the resonator as in the figure below:

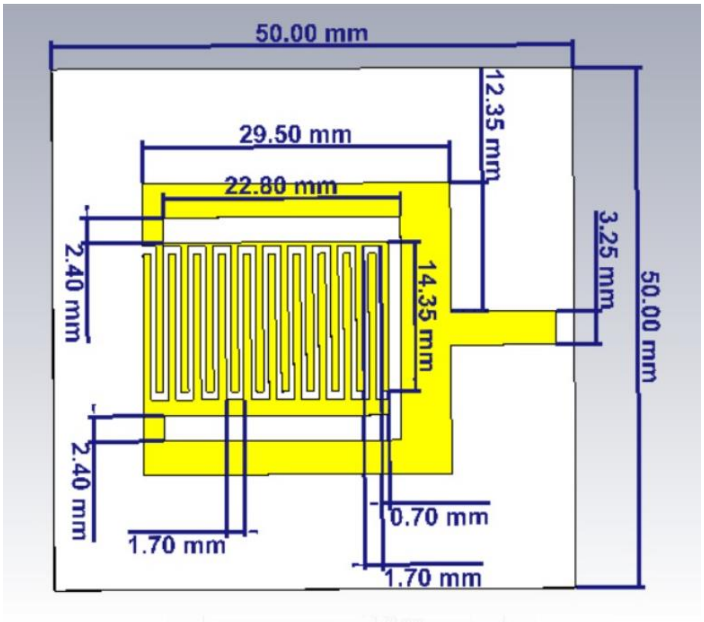

Figure4-16:Simulation and optimization were performed using CST Microwave Studio The dimensions are detailed in the previous image.

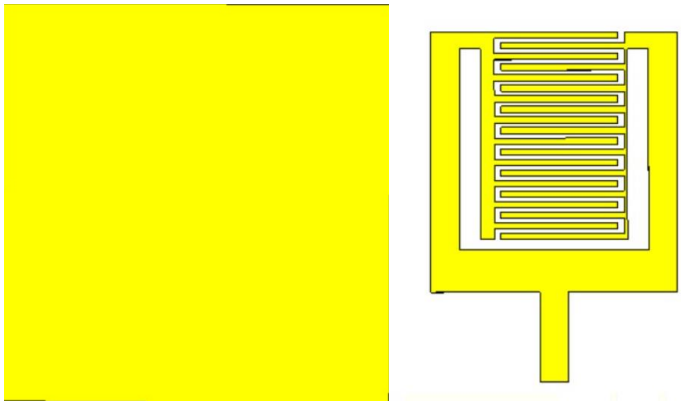

Figure4-17: (a) and (b) : Stepped Impedance Resonator Sensor model in CST.

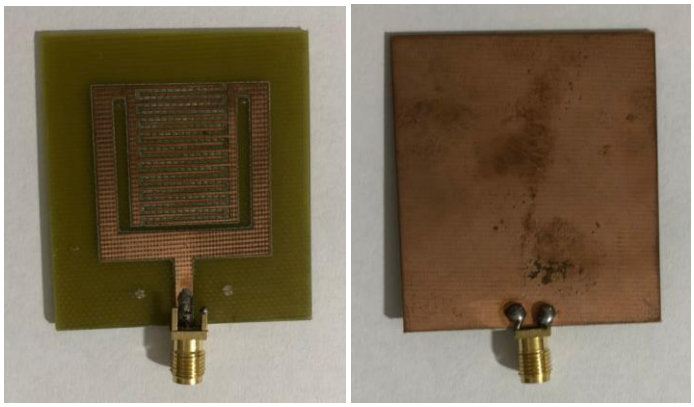

Figure4-18:The fabricated of Stepped Impedance Resonator Sensor.

The effect of microwaves on the human body:

The interaction between Microwave waves and the human body primarily involves the heating effect of microwaves on tissues, as microwaves are a form of non-ionizing electromagnetic radiation. When microwaves encounter water molecules in food or biological tissues, they cause the molecules to vibrate, generating heat

Here are some key points regarding the effects of microwaves on the human body:

Tissue Heating: The primary effect of Microwave waves on the human body is the heating of tissues. This occurs when microwaves are absorbed by water molecules in the body, leading to an increase in molecular motion and, consequently, an increase in temperature.

Thermal Burns: Prolonged or intense exposure to Microwave waves can potentially lead to thermal burns. However, Microwave waves are designed to prevent excessive leakage of Microwave waves, and when used properly, the levels of exposure are considered safe.

Superficial Heating: Microwaves tend to heat tissues near the surface of the body more than deeper tissues. The skin and outer layers of tissue absorb microwaves more readily.

Safety Standards: International safety standards regulate the design and manufacturing of Microwave waves to ensure that they meet specific criteria for limiting microwave leakage. When Microwave waves are used according to these standards and guidelines, the exposure to Microwave waves is typically well below levels that would cause harm.

Non-Ionizing Nature: Unlike ionizing radiation, which has sufficient energy to ionize atoms and molecules, microwaves do not have the energy required to cause ionization. This non-ionizing nature of Microwave waves that they do not have the ability to directly damage DNA or cause genetic mutations.

What is a microwave and what are the specifications of the wave capable of penetrating the human body?

A microwave is a type of electromagnetic radiation with wavelengths ranging from about one millimeter to one meter, falling between radio waves and infrared radiation in the electromagnetic spectrum. Microwaves are commonly used for various purposes, including communication (microwave ovens, radar, and satellite communication) and scientific and medical applications.

In terms of penetration into the human body, microwaves are generally non-ionizing radiation, meaning they do not have sufficient energy to remove electrons from atoms or molecules (ionization). Instead, microwaves primarily interact with water molecules, and their penetration into biological tissues is limited. The depth of penetration depends on factors such as the frequency of the microwaves and the characteristics of the tissues.

When and how is the skin affected by microwave waves?

Tissue Mimicking Model:

Four-layer human tissue models with five different glucose concentrations were fabricated to test the efficiency and practicality of the resonators. The resonator performance with these tissue models is provided in both simulation (using ANSYS HFSS) and in measurement. This four-layer tissue modeling. The properties of this four-layer tissue model were rigorous measured and verified to accurately model human tissue in that paper.

The permittivity and conductivity of these layers are needed for ANSYS HFSS simulations. Since the changes in properties were not significant from 2 GHz to 2.4 GHz, the same properties were used for all three designs (Color:Micro USB with cabal .SEN-

SENSOR .arduino). Properties of each layer are provided in Table 4.4, which were obtained from a broadband frequency measurement. The material and procedure for tissue modeling were Use the measured properties from that work

Table 4.4. Properties of each layer at 2 to 2.4 GHz frequency range:

Tissue Type	Permittivity	Conductivity (S/m)
Wet Skin	43.5	1.2
Fat	5.28	0.103
Blood (0 g dextrose)	59.5	2.5
Blood (0.14 g dextrose)	58.5	2.5
Blood (0.24 g dextrose)	57	2.5
Blood (0.34 g dextrose)	55.5	2.5
Blood (0.44 g dextrose)	54	2.5
Muscle	53	1.5

The conductivity and permittivity of the simulated four-layer tissue model from 0 to 20 GHz is Since the electromagnetic field of the resonators changes by placing a material with relative permittivity greater than 1 close to it, the expectations for the ring resonator and CCSR are to see a change in their responses by placing tissues with different properties (which corresponds to different glucose index).

Chapter5:

Methodology:

Non-invasive glucose monitoring is a critical area of research aimed at providing a convenient and pain-free method for monitoring blood glucose levels. In this methodology section, we outline the procedures and techniques for developing a non-

invasive glucose monitoring system utilizing the Spectral Triad NIR sensor (AS7265x) and the NanoVNA V2 3G micro resonant.

project Design:

Our research employs a multifaceted design that integrates experimental, observational, and real-time monitoring components:

Experimental Component: Our study incorporates an experimental approach to investigate the feasibility and accuracy of non-invasive glucose monitoring. We will conduct controlled experiments using the Spectral Triad NIR sensor (AS7265x) and the NanoVNA V2 3G micro resonant. These experiments involve controlled variations in glucose levels using standardized glucose solutions. This component focuses on collecting spectral and resonant data under controlled conditions.

Real-Time Monitoring (GSM Module): Additionally, our research includes real-time monitoring through the integration of a GSM module. This feature enables continuous data transmission and remote monitoring of glucose levels, offering a valuable perspective on the system's performance in real-time scenarios.

NIR Spectroscopy Equipment:

We will utilize the Spectral Triad NIR sensor (AS7265x) for the collection of near-infrared spectral data. This sensor features six discrete spectral channels, allowing us to capture a wide range of wavelengths and spectral information relevant to glucose monitoring. The sensor will be integrated into the monitoring device, positioned appropriately for optimal measurement accuracy.

SparkFun Triad Spectroscopy Sensor (AS7265x (Qwiic)):

The SparkFun Triad Spectroscopy Sensor is a powerful optical inspection sensor. Three AS7265x sensors are combined alongside a visible, UV, and IR LEDs to illuminate and test various surfaces for light spectroscopy. We can interface AS7265x with Arduino & any other microcontroller. Using the Triad Spectroscopy Sensor AS7265x, we can make our own Spectrophotometer. The sensor has the ability to measure and characterize how various types of materials absorb or reflect 18 different frequencies of light ranging from

410nm to 940nm. The AS72651, combined with the AS72652 (spectral response from 560nm to 940nm) and the AS72653 (spectral response from 410nm to 535nm) form an AS7265x 18-channel multi-spectral sensor chip-set.

Figure 5-1: SparkFun Triad Spectroscopy Sensor - AS7265x (Qwiic)

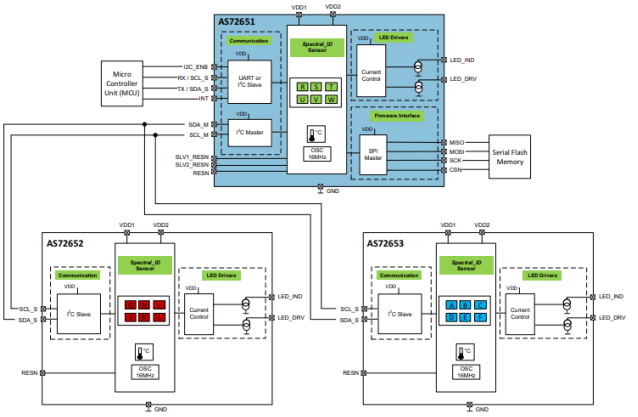

Figure 5-2: AS7265x Chip-Set Block Diagram

The compact and durable AS7265x device features a 20-pin Land Grid Array (LGA) package measuring 4.5mm x 4.7mm x 2.5mm, ensuring a small form factor while offering robust performance. Additionally, it operates seamlessly within a wide temperature range spanning from -40°C to 85°C, making it suitable for a variety of environmental conditions. Furthermore, it boasts a built-in aperture for enhanced functionality.

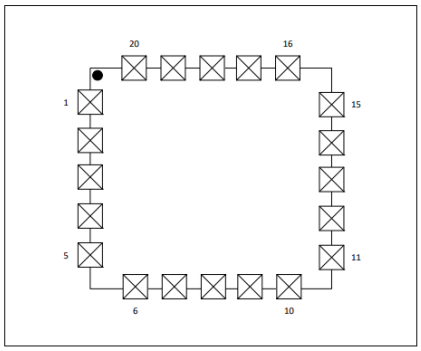

Figure 5-3: Pin Diagram of AS7265x (Top View)

Electrical Characteristics:

All limits are guaranteed with VDD = VDD1 = VDD2 = 3.3V, TAMB = 25°C. The parameters with min and max values are guaranteed with production tests or SQC (Statistical Quality Control) methods. VDD1 and VDD2 should be sourced from the same power supply output.

Hardware Overview:

Sensors:

The AS7265x is the simplest Triad Spectroscopy Sensor from Sparkfun which can also be called a Spectrophotometer. The sensor is formed by combining three sensors AS72651, AS72652 & AS72653. The AS72651 is for measuring the visible light spectrum. Similarly, AS72652 is for measuring UV Light. The AS72653 is an IR Sensor for measuring IR Radiation. The sensor also has a 4Mbit EEPROM which is loaded by the firmware which drives the system. The EEPROM is read by the AS72651 at power on.

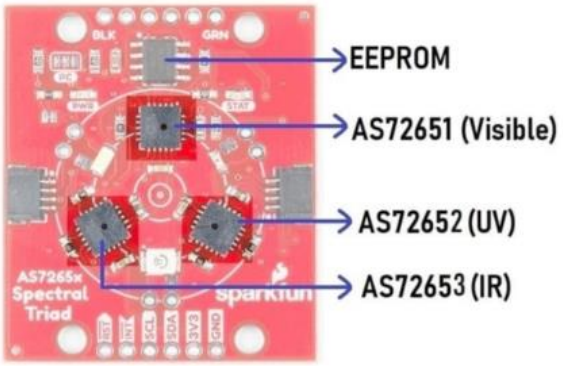

Figure 5-4:

The AS72651 communicates with the x2 and x3 sensors over a dedicated I2C bus (the AS72651 is the master, the AS72652 and AS72653 are slaves). The AS72651 combines its sensor data with the data from the x2 and x3 sensors and exposes the datums to the user as a single array of registers. The SparkFun AS7265x Spectral Library makes it seamless to read any of the 18 frequencies of sensing.

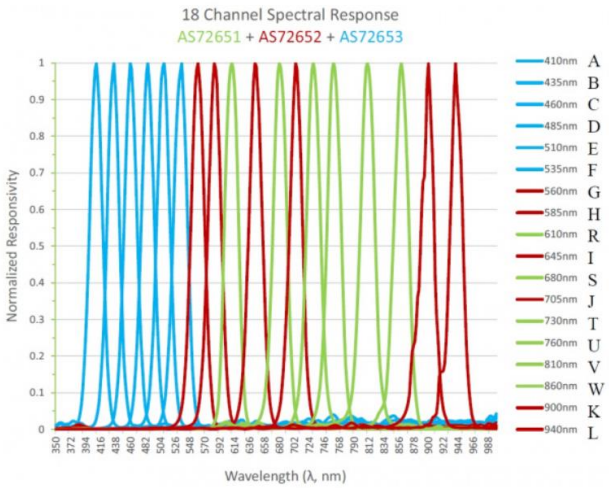

Figure 5-5: AS7265x 18-Channel Spectral Responsivity

The AS7265x Triad Spectroscopy Spectral Sensor detects the light from a wavelength of 410nm to 940nm. The sensor has the ability to measure 18 individual light frequencies with precision down to 28.6 nW/cm2 and accuracy of +/-12%. The sensor operates at a typical voltage of 3.3V. The sensor has I2C pins as SDA (Serial Data) & SCL (Serial Clock) with an I2C address of 0x49. The default baud rate for the sensor is 115200.

Overall This component offers seamless integration into existing systems, as it eliminates the need for extra signal conditioning. It features a 16-bit ADC with accessible digital control, programmable LED drivers, and supports a voltage range of 2.7V to 3.6V with a user-friendly I²C interface, making it versatile and easily adaptable to various applications.

UART Interface:

AS72651 has an UART interface to communicate to the controller. AT commands can be used for data acquisition, sensors configuration, and LED drivers control. Please refer to AS72651 data sheet for complete AT commands. Pin11 of AS72651 is the RX of UART, which AS72651 receives the information from the controller. Pin12 of AS72651 is the TX

of UART, which AS72651 transmits the information to the controller. Any Windows terminal application with baud rate 115200, 8 data bit, 1 stop bit, and none parity can be used for AT commands. Since pin11 and pin12 of AS72651 are also shared with I2C interface, the pin8, I2C_ENB, has to be pulled down for UART interface configuration.

I2C Interface:

AS72651 has both I2C master and I2C slave interface. Both support I2C fast mode (400 KHz) and standard mode (100 KHz). AS72651 I2C slave interface is used for communication to the controller. The pin11, SCL_S, is assigned to the I2C bus clock and the pin12, SDA_S, is for the bus data. The pin8, I2C_ENB, has to be pulled HIGH.

AS72651 I2C master interface is used for controlling AS72652 and AS72653. The pin20, SCL, is the I2C bus clock and the pin1, SDA, is for the I2C bus data. The communication between AS72651 and AS72652/AS72653 is managed by the firmware. According to I2C specification, both SCL and SDA are open drain and need to be connected to a positive supply voltage via a pull-up resistor. The pull-up resistors, R13/R14 in the typical schematic, pull the line high when it is not driven low by the open drain interface. The maximum value of the pullup resistor is limited by the bus capacitance, C_b, and the rise time, t_r, as below.

$$R_{p(max)}=\frac{tr}{0.8473*Cb}$$

The bus capacitance is the total capacitance of wire, connections, and pins. I2C Bus specifies the maximum rise time is 300ns. On the other hand, the minimum value of the pull-up resistor depends on the device logical specifications and allows V_{OL} level to be read as a valide logical low.

$$R_{p(min)}=\frac{Vdd-VOL(max)}{IOL}$$

For the AS7265x Multispectral Chipset application with 3.3V supply voltage, 0.4V maximum V_{OL}, and the specified minimum sink current of 3mA for standard mode (100 KHz) or fast mode (400 KHz), the minimum pull-up resistor value is 966.7Ω. Then the decision of the pull-up resistor value would be based on the rise time, the total bus capacitance, and the power budget. A smaller resistor may get short rise time but has higher power consumption.

LEDs/Bulbs on AS7265x Sensor:

The sensor contains 3 diifferent LED, i.e white LED (5700K), UV LED (405nm) & IR LED (875nm). The main purpose of these LEDs is to illuminate the targeted object with the largest swath of visible or invisible light.

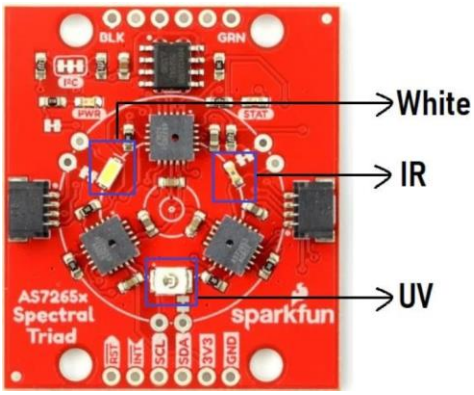

Figure 5-6: LEDs/Bulbs on AS7265x Sensor

Apart from the 3 illumination LEDs, the sensor has a power LED and a status LED. The blue status LED indicates various states of the AS72651 sensor. This LED can be disabled through the SparkFun library. The red power LED is provided to indicate the board is properly powered up or not.

Light Source Selection:

The Figure bellow shows AS7265x Multispectral Chipset generic application. AS7265x chipset produce the sensor output data based on the received reflection light rays from the target. The light source selection would be dependent on the spectral responsivity of reflected light and characteristics of the target. For example, if the target is expected to absorb 610nm light in visible range and the applicationneeds to distinguish the target from others, a broadband white LED might be used as the light source for AS7265x and AS7265x 610nm channel should be checked. Various applications may requireN different light sources in our case we will use 940nm light in NIR range.

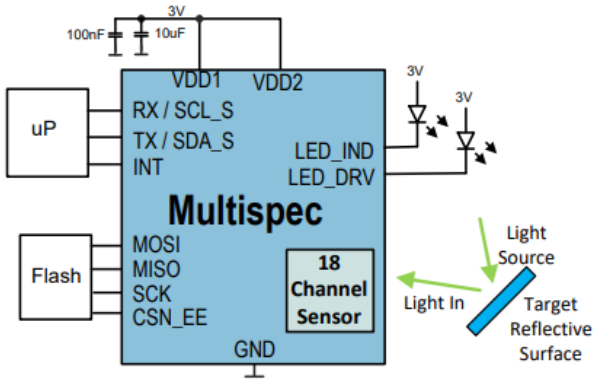

Figure 5-7:

Optic Considerations :

Each AS7265x device has an open aperture on the surface. The diameter is 0.75mm and the package field of view is ±20.5°. The light rays in the range as shown in bellow figure would arrive at the sensor. Since AS7265x Multispectral Chipset consists of three AS7265x devices, an external optical device might be needed so incident rays to each device is same. As an open-aperture device, precautions must be taken to avoid particulate or solvent contamination as a result of any manufacturing processes, including pick and place, reflow, cleaning, integration assembly and/or testing.

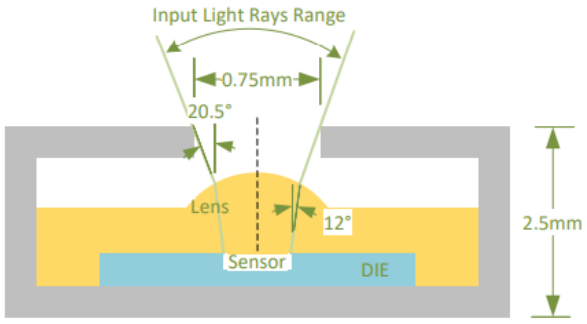

Figure 5-8:AS7265x LGA Average Field of View

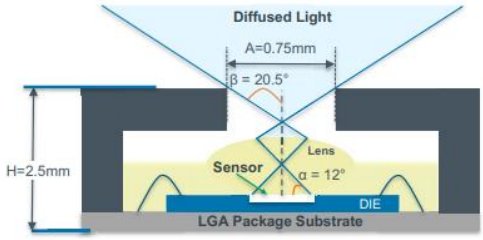

Figure 5-9:AS7265x LGA Average Field of View

Features and Register Structure:

AS72651 supports I2C both standard mode and fast mode. The addressing mode is 7+1-bit so when the controller send a read command to AS72651, the salve address plus R/W bit should be 0x93 and when sending a write command, it should be 0x92. Both read and write are single byte process.

GSM:

GSM (Global System for Mobile communications) is an open, digital cellular technology used for transmitting mobile voice and data services. GSM supports voice calls and data transfer speeds of up to 9.6 Kbit/s, together with the transmission of SMS. GSM uses narrowband TDMA, which allows eight simultaneous calls on the same radio frequency. In the traditional GSM, data transmission is done using Circuit Switched Data (CSD) technique whereby the network allocates one radio channel to a MS when data is to be transmitted to the network and the radio channel remain occupied for the con Network structure The network is structured into a number of discrete sections:

• Base Station Subsystem – the base stations and their controllers

explained

• Network and Switching Subsystem – the part of the network most similar to a fixed network, sometimes just called the "core network"

• GPRS Core Network– the optional part which allows packet-based 22 Internet connections

• Operations support system (OSS) – network maintenance

GSM is a cellular network, which means that cell phones connect to it by searching for cells in the immediate vicinity. There are five different cell sizes in a GSM network—

macro, micro, pico, femto, and umbrella cells. The coverage area of each cell varies according to the implementation environment. Macro cells can be regarded as cells where the base station antenna is installed on a mast or a building above average rooftop level. Micro cells are cells whose antenna height is under average rooftop level; they are typically used in urban areas. Picocells are small cells whose coverage diameter is a few dozen metres; they are mainly used indoors. Femtocells are cells designed for use in residential or small business environments and connect to the service provider's network via a broadband internet connection. Umbrella cells are used to cover shadowed regions of smaller cells and fill in gaps in coverage between those cells. Cell horizontal radius varies depending on antenna height, antenna gain, and propagation conditions from a couple of hundred meters to several tens of kilometers. The longest distance the GSM specification supports in practical use is 35 kilometers (22 mi). There are also several implementations of the concept of an extended cell, where the cell radius could be double or even more, depending on the antenna system, the type of terrain, and the timing advance. Indoor coverage is also supported by GSM and may be achieved by using an indoor Pico cell base station, or an indoor repeater with distributed indoor antennas fed through power splitters, to deliver the radio signals from an antenna outdoors to the separate indoor distributed antenna system. These are typically deployed when significant call capacity is needed indoors, like in shopping centers or airports. However, this is not a prerequisite, since indoor coverage is 23 also provided by in-building penetration of the radio signals from any nearby cell.

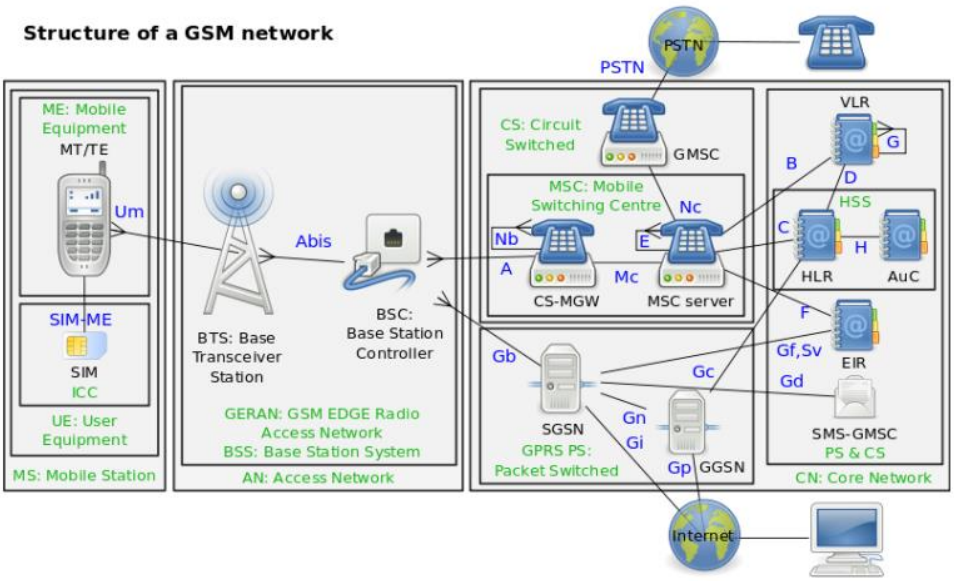

Figure 5-10: structure of a GSM network

GSM Network:

In this project, I will utilize the SIM900A as the GSM module to implement the communication infrastructure. Global System for Mobile Communication (GSM) was used to receive the information signal from the microcontroller and send it to a mobile application. To facilitate real-time monitoring and data transmission, we will integrate GSM (Global System for Mobile Communications) technology into our system, employing the SIM900A module. This technology will enable the secure and efficient transmission of glucose measurements to a designated platform. Users and healthcare providers will access these measurements remotely, ensuring timely intervention and monitoring. The SIM900A's capabilities in GSM communication make it an integral component for establishing reliable and efficient connections in our healthcare monitoring project.

SIM 900A Modul:

SIM 900A is GSM / GPRS module which is used to send message or phone. SIM900A features Quad Band 850/900/1800/1900 MHz and can be used on GSM networks in various countries, GPRS multi-slot class 10/8, GPRS mobile station Class B, Compliant to GSM Phase 2/2 +, Class 1 (1 W (AT) 1800/1900 MHz), Command AT Command - Standard Commands: GSM 07.07 & 07.05, Enhanced Command: SIMCOM AT Commands. Short Message Service (SMS), Embedded TCP / UDP Stack, RTC Support, Serial Port Selection (3.3 Volts and 5 Volts), There are Jack speakers and Headphones (on certain breakout board types), Low power consumption - 1.5mA (Sleep mode), and working at a temperature of -40 c to +85 C. SIM900A module is shown in figure 5-11.

Figure 5-11: SIM900A Module

Figure 3 shows the module SIM900A antenna version, in this mode do not use adapter power supply. Shape and specification of SIM 900A module as shown in figure 3. but SIM 900A module has input specification different outputs, at the input of the sim900a

module I use using the VCC Pin input, Data, and GND, but there is a Module version SIM900A using RS232 output input type and adapter power supply of 9-12 Volt DC depending on SIM900A series used. for more details, SIM900A Module is described in the schematic on figure 5-12.

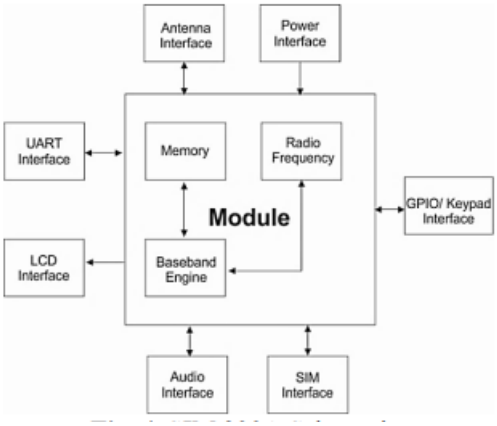

Figure 5-12: SIM 900A Schematic.

SIM900 Functional Diagram:

The following figure shows a functional diagram of the SIM900 and illustrates the mainly functional part:

- The GSM baseband engine
- Flash and SRAM
- The GSM radio frequency part
- The antenna interface
- The Other interfaces

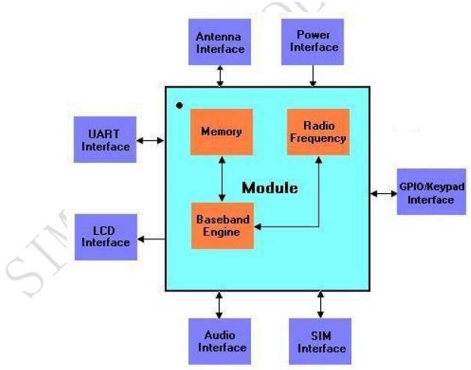

Figure 5-13: SIM900 functional diagram

SIM900A pinout:

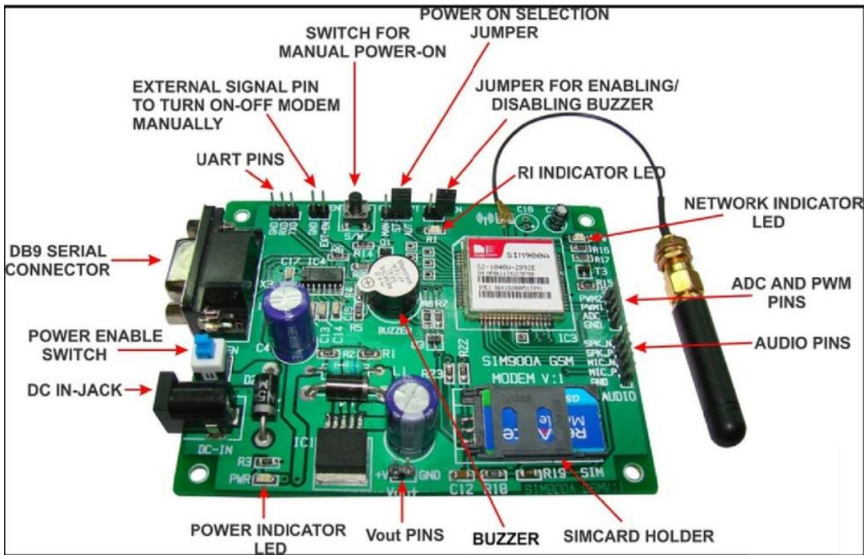

Figure 5-14: SIM900A pinout

1.DC IN Jack: DC Input PIN for GSM MODEM.

2.Power Enable Switch: This is Power enable switch to Turn ON or turn OFF power to the board. When pressed turns ON the board and when released turns OFF the board

3.Power Indicator LED: Modem power indicator LED.

4.EXT-EN: External enables pin to turn ON or OFF SIM900A module with external controlling circuit.

5.S/W: Onboard switch to turn ON or OFF SIM900A module manually.

6.Power ON selection jumper: To select the power ON mode of the SIM900A (Manual or Automatic)

7.RI LED and Buzzer: Incoming message and call indicator LED and buzzer.

Power Supply:

The power supply of SIM900 is from a single voltage source of VBAT=3.4V…4.5V. In some case, the ripple in a transmitting burst may cause voltage drops when current consumption rises to typical peaks of 2A. So the power supply must be able to provide sufficient current up to 2A.

For the VBAT input, a local bypass capacitor is recommended. A capacitor (about 100μF, low ESR) is recommended. Multi-layer ceramic chip (MLCC) capacitors can provide the

best combination of low ESR and small size but may not be cost effective. A lower cost choice may be a 100μF tantalum capacitor (low ESR) with a small (0.1 μF to 1 μF) to ceramic in parallel, which is illustrated as following figure. The capacitors should be placed as close as possible to the SIM900 VBAT pins. The following figure is the recommended circuit.

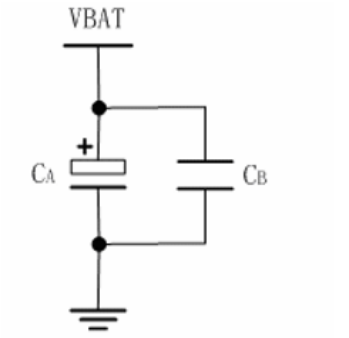

Figure 5-15: Reference circuit of the VBAT input

The circuit design of the power supply depends strongly upon the power source where this power is drained. The following figure is the reference design of +5V input source power supply. The designed output for the power supply is 4.1V, thus a linear regulator can be used. If there's a big difference between the input source and the desired output (VBAT), a switching converter power supply will be preferable because of its better efficiency especially with the 2A peak current in burst mode of the module.

The single3.6 VLi-Ion cell battery type can be connected to the power supply of the SIM900 VBAT directly. But theNi_Cd or Ni_MH battery types must be used ,since their maximum voltage can rise over the absolute maximum voltage for the module and damage it.

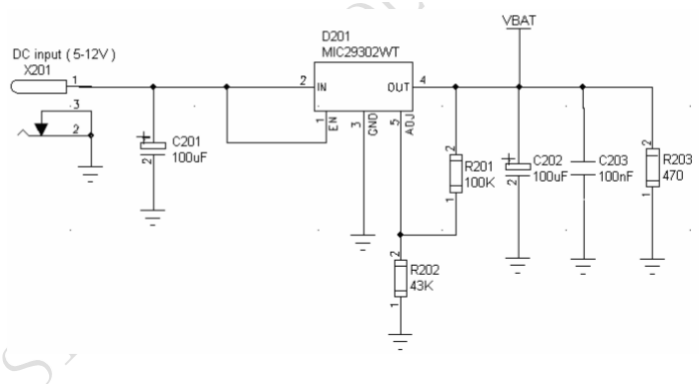

Figure 5-16: Reference circuit of the source power supply input

Additionally, the VBAT voltage ripple wave during maximum power transmit phases should be considered. Test conditions typically include a VBAT of 4.0V, maximum output

current of 2A, a 100µF tantalum capacitor CA (with ESR of 0.7Ω), and a 1µF ceramic capacitor CB.

These considerations ensure a stable and reliable power supply for the SIM900 module, critical for its proper functioning in various operating conditions.

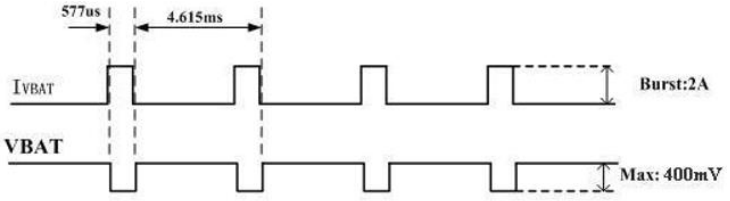

Figure 5-17: VBAT voltage drop during transmit burst

Microcontroller:

A microcontroller is a compact integrated circuit that contains a processor core, memory, and programmable input/output peripherals. It serves as the brain of electronic devices, executing programmed instructions to control various functions. Microcontrollers are commonly employed in a myriad of applications, ranging from simple embedded systems to sophisticated gadgets. In our project, we will harness the capabilities of the Arduino Mega, a powerful microcontroller board. With its ample input/output pins, versatile communication interfaces, and expanded memory, the Arduino Mega provides us with a robust platform to develop and control our electronic systems effectively.

The Arduino Mega is a versatile microcontroller board that we will employ for various electronic projects. With its extensive range of input and output pins, the Mega offers a robust platform for interfacing with sensors, actuators, and other components. Its 54 digital I/O pins, 16 analog inputs, and multiple communication interfaces, including UART, I2C, and SPI, make it suitable for a wide array of applications. The Mega's enhanced capabilities, such as a larger flash memory and RAM compared to other Arduino boards, enable the implementation of complex algorithms and handling of substantial data. Whether we are creating interactive installations, robotics, or monitoring systems, the Arduino Mega serves as a reliable and powerful foundation for bringing our electronic ideas to life. Its open-source nature and extensive community support further contribute to the accessibility and flexibility of our projects.

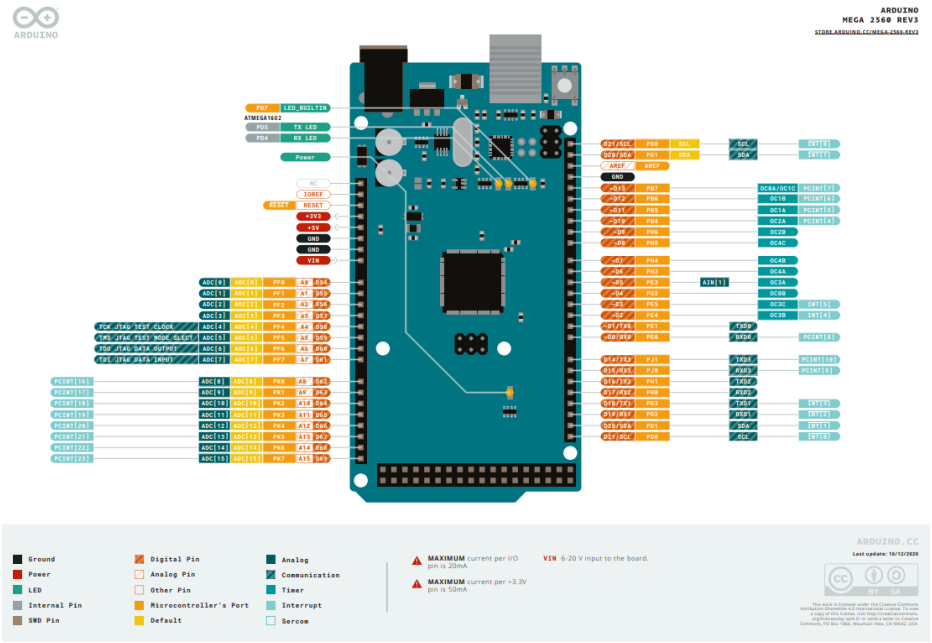

Figure 5-18: Arduino Mega Pinout

Summary:

Microcontroller	ATmega2560
Operating	Voltage 5V
Input Voltage (recommended)	7-12V
Input Voltage (limits)	6-20V
Digital I/O Pins	54 (of which 14 provide PWM output)
Analog Input	Pins 16
DC Current per I/O Pin	40 mA
DC Current for 3.3V Pin	50 mA
Flash Memory	256 KB of which 8 KB used by bootloader
SRAM	8 KB
EEPROM	4 KB
Clock Speed	16 MHz

Power:

The Arduino Mega can be powered via the USB connection or with an external power supply. The power source is selected automatically. External (non-USB) power can come either from an AC-to-DC adapter (wall-wart) or battery. The adapter can be connected by plugging a 2.1mm center-positive plug into the board's power jack. Leads from a battery can be inserted in the Gnd and Vin pin headers of the POWER connector. The board can operate on an external supply of 6 to 20 volts. If supplied with less than 7V, however, the 5V pin may supply less than five volts and the board may be unstable. If using more than 12V, the voltage regulator may overheat and damage the board. The recommended range is 7 to 12 volts.

NanoVNA V2 3G Micro Resonant:

The NanoVNA V2 3G micro resonant plays a crucial role in our data collection process. This device measures resonant characteristics of sensing elements, and changes in these characteristics will be correlated with glucose levels. The NanoVNA V2 3G will be used to capture resonant data during controlled experiments and real-world observations.

VNA basics:

Vector Network Analyzer (VNA) is the most commonly used instrument in the field of RF and microwave, VNA measures the reflection and transmission behavior of a device under test (DUT) across a configured frequency range. VNA is usually used to measure antenna impedance, cable Nano VNA-F V2 is a dual-port portable vector network analyzer that can be used to measure the S11 parameters of a single-port network, or to measure the S11 and S21 parameters of a dual-port network. If you need to measure the S22 and S12 parameters of the dual-port network, you can achieve it by exchanging the measurement ports. It uses our new VNA-R architecture featuring temperature drift cancellation and reduced crosstalk, showing no visible drift in all indoor conditions. No noticeable drift, allowing calibrations to be kept for > 3 months (compared to < 30 minutes for other low cost VNAs). Improved shielding and all-aluminum enclosure of the NanoVNA V2 Plus4 increases its dynamic range to >90dB, achieving similar results as professional VNAs, and allows measuring duplexers. TDR / Time Domain measurements allow testing cable length and discontinuities. Improved USB protocol allows full speed streaming of measured data to the PC. VNA must be calibrated before any measurements are performed. Details as it appears in the following figure

Figure 5-19: Job NanoVNA V2 3G in the project:

The sensor sends the signal and then the Arduino (controller) receives it. It receives the signal, reads and processes it, and then sends it to NanoVNA V2 3G. reads the signal received from the Arduino and analyzes it and takes the blood glucose rate, as this depends on the frequency, polarity and wavelength.

Main screen:

Figure 5-20: Main screen

- START frequency: The start frequency is shown in this area.
- STOP frequency: The stop frequency is shown in this area.
- Marker: Up to 4 markers can be displayed at the same time.

The active marker can be moved to any of the measured points in the following 2 ways:

1. Push the UP or DOWN buttons.
2. Drag the marker on the touch panel (recommend to operate with a stylus).

- Calibration status:

O: Indicates OPEN calibration has been performed.

S: Indicates SHORT calibration has been performed.

L: Indicates LOAD calibration has been performed.

T: Indicates THROUGH calibration has been performed.

C: Indicates that the device has performed a calibration.

*: Indicates that the calibration data has not been stored and will be lost when power off.
c: Indicates that the calibration data is Interpolated.

Cn: Indicates that the corresponding calibration data is loaded (7 sets from 0 to 6).

- Reference position

Indicates the reference position of the corresponding trace. You can change the position by:

【DISPLAY】→【REF POS】

- Marker Table

Up to 4 sets of marker information can be displayed at the same time, each set of marker

Information includes frequency and 2 other parameters.

The diamond mark in front of the marker table indicates which is the active marker.

You can open, select or close a marker by:

【MARKER】→【SELECT】→【MARKER】

To quickly activate a marker, you can tap on the frequency value region of the corresponding row

of the marker table (recommend to operate with a stylus).

It is possible to move the marker table up and down by:

【MARKER】→【SELECT】→【POSITION】

The marker table can be dragged when tap down and holding the measured value area of the

marker table for more than 0.5 seconds;

If you want to save the setting of marker table display position, you can do it by:

【RECALL/SAVE】→【SAVE】→【SAVE n】

- Trace status box

The status of each trace format and the value corresponding to the active marker are displayed.

For example, if the display is showing: S21 LOGMAG 10dB/ 0.03dB, read it as follows:

The cyan trace is currently active

Channel: PORT2 (transmission)

Format: LOGMAG

Scale is 10dB/div

S21 value at current frequency is 0.03dB

Tap on any set of trace status box will activate the corresponding trace.

If the trace is active, tap on the specific region of the trace status box will trigger shortcuts

Tap on “channel” region (e.g., S21) will quickly switch channel;

Tap on “format” region (e.g., LOGMAG) will quickly open the FORMAT menu;

Tap on “scale” region (e.g., 10dB/) will quickly open SCALE and REFERENCE POSITION menu.

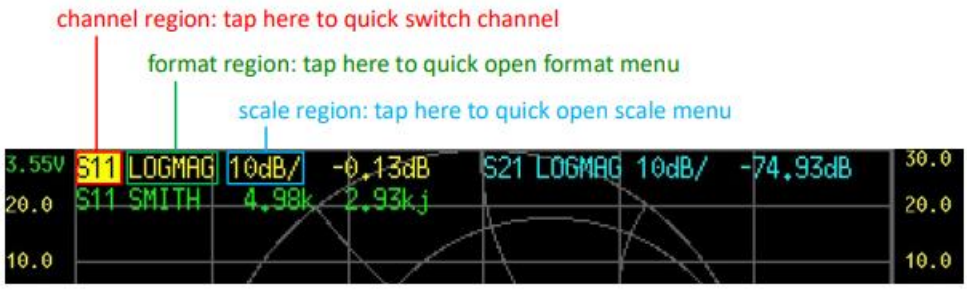

Figure 5-21: Main screen

Battery voltage: The voltage of the built-in lithium battery is shown here. If the battery voltage is lower than 3.3V,

Please charge the device.

- Left ordinate: The left ordinate always shows the scale label of trace 0.Tap on the area of left ordinate to quickly set the scale of trace to 0.
- Right ordinate: The right ordinate always shows the scale label of current active trace. Tap on the area of the right ordinate to quickly set the scale of current active trace.
- Sweep points: Show sweep points

(CALIBRATE): Tap on (CALIBRATE) to enter the calibration interface, and perform the calibration accordingly

to the following steps

STEP 1: Connect the OPEN kit to PORT1 or the end of the cable connected to PORT1, as shown in the figure below:

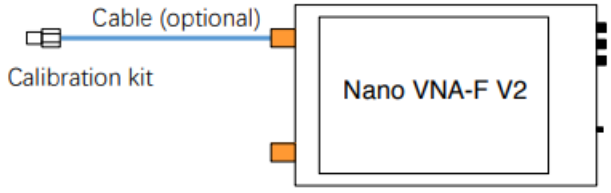

Figure 5-22:

STEP 2: Connect the SHORT kit to PORT1 or the end of the cable connected to PORT1, tap on (SHORT)

to complete the short calibration

STEP 3: Connect the LOAD kit to PORT1 or the end of the cable connected to PORT1, tap on (LOAD) to complete the load calibration.

STEP 4: Connect PORT1 and PORT2 with cable and adapter (optional), as shown in the figure below, then tap on (THROUGH) to complete the through calibration.

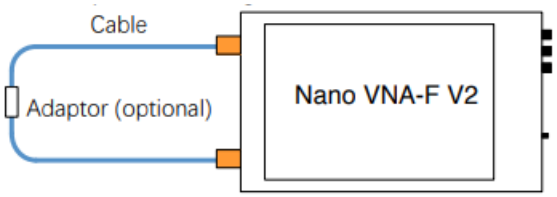

Figure 5-23:

Figure 5-24: Display screen of the VNA.

Usually we need to connect the DUT to VNA with cables, at this time, the cable becomes a part of the measurement system, and the end of the cable should be treated as the VNA port during calibration Nano VNA-F V2 supports automatic calculation of L/C matching parameters, matching the load impedance to the source 50ohm impedance

The structure of L/C matching network is shown in the figure below: Series:

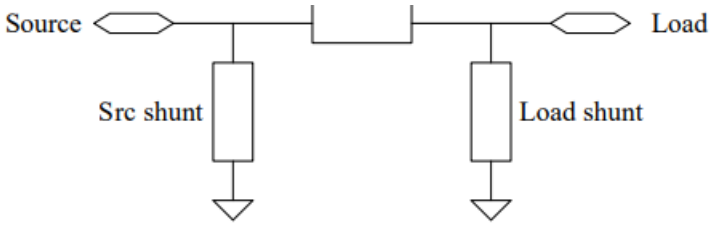

Figure 5-25: The structure of L/C matching network

Specifications:

Parameter	Board version	Specification	Conditions
Frequency range	V2_2, V2 Plus	50kHz - 3GHz	-
	V2 Plus4, V2 Plus4 Pro	**50kHz – 4.4GHz**	-
Frequency resolution	All	0.01MHz	-
System dynamic range (calibrated)	V2_2, V2 Plus	60dB	
	V2 Plus4	**90dB**	AVG=20, 1GHz
	V2 Plus4 Pro	**90dB**	BW=1.6kHz, AVG=5, 1GHz
		96dB	BW=1.6kHz, AVG=20, 1GHz
S11 noise floor (calibrated)	All	-50dB	f < 1.5GHz
		-40dB	f < 3GHz
Sweep points	V2 Plus4	1 – 1024 points (with NanoVNA-QT software). More points (up to 65535) are possible depending on the performance of your PC.	-
Sweep time	V2 Plus4	0.25s	Default sweep settings
	V2 Plus4 Pro	0.16s	Default sweep settings BW=10kHz
Power supply	All	USB, 4.6V – 5.5V	-

Parameter	Board version	Specification	Conditions
Supply current	All	500mA typ	No charging
Battery current, charging	All	1.2A typ	-
Battery capacity	V2 Plus4, V2 Plus4 Pro	3200mAh	-
Operation ambient temperature	All	0℃ - 45℃ *	* by design, not tested in production
Ambient temperature during battery charging	All	10℃ - 45℃	-

Hardware Architecture:

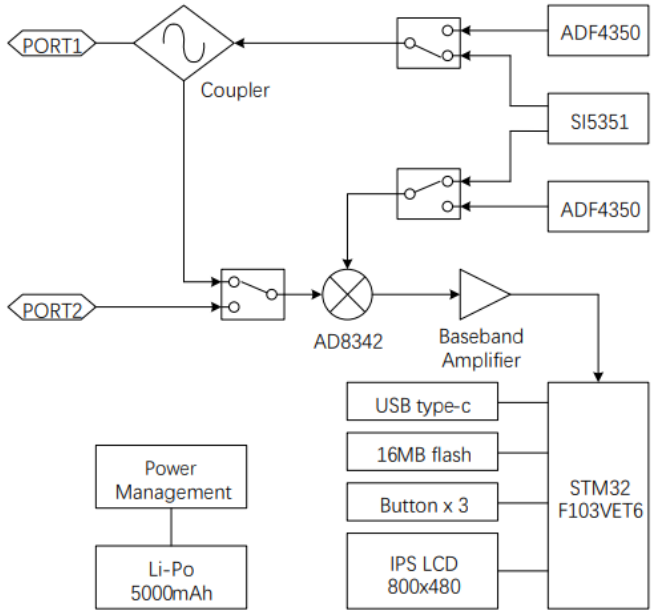

Figure 5-26: Hardware Architecture

Power source for the device:

For my graduation project, the NIR-based blood glucose measurement device will be powered using a 2 Amp, 12 Volt power adapter. This adapter ensures a stable and sufficient power supply to the device, facilitating

accurate and reliable operation. By providing consistent power, the 2 Amp adapter helps maintain the optimal performance of the NIR-spectroscopy swnsor and the associated electronic components, ensuring precise measurement of glucose levels in the blood.

Figure 5-27: 12 Volt 2 Amp AC Adaptor.

Chapter6:

Experimental setup:

1. **Experimental setup OF non-invasive glucose monitoring system base on NIR spectroscopy:**

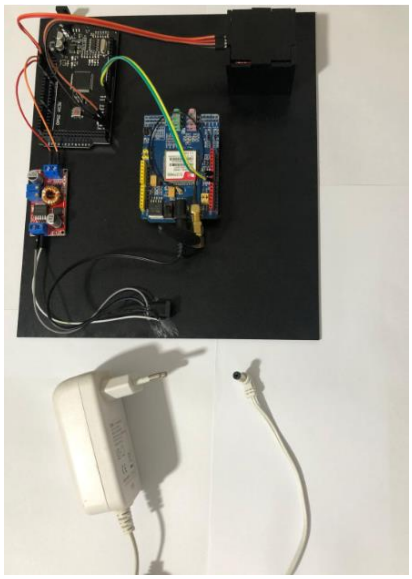

Figure6-1:the setup of the non-invasive glucose monitoring system

the setup of the non-invasive glucose monitoring system based on NIR spectroscopy depicted in figure 6-1.

The figure shows the arduino connected to the gsm module and the as7265x sensor and fed through a step-down convertor that is fed using a power adapterو The GSM module is also fed directly from power adapter.

2. Experimental setup OF non-invasive glucose monitoring system base on Microstrip resonator

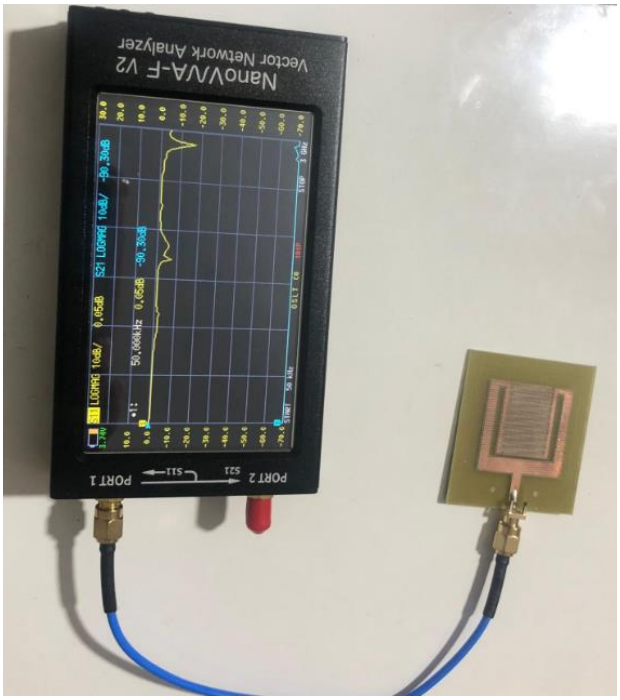

Figure6-2:the setup of non-invasive glucose monitoring system base on Microstrip resonator.

Chapter7:

Results

NIR spectroscopy results:

We took samples using a traditional blood sugar testing device, then compared them to the results of a non-invasive glucose monitoring system based on NIR spectroscopy. The results are as shown in the following table.

Table7-1:

Sample number	645nm result	860nm result	940nm result	The result of the traditional diabetic device(mg/dL)
1	12.2	36.9	313.15	310

2	17.6	34.2	393.64	277
3	13.21	40	279.64	354
4	10	44	310	315
5	52	20	501	126
6	23.4	45	640	92
7	13.9	40	400	254
8	30	35	380	284
9	27	41	666	89
10	95	110	350	450
11	90	67	497	155
12	45	58	592	84
13	51	50	673	79
14	30	52	587	66
15	18	45	437	146
16	20	51	530	75
17	16	33	582	82

We used polynomial regression to formulate a relationship linking the original blood glucose reading using the traditional device and the blood glucose reading of non-invasive glucose monitoring system base on NIR spectroscopy.

We used MATLAB to find using polynomial regression the best-fit equation and plot the curve and the results as shown in the following figure.

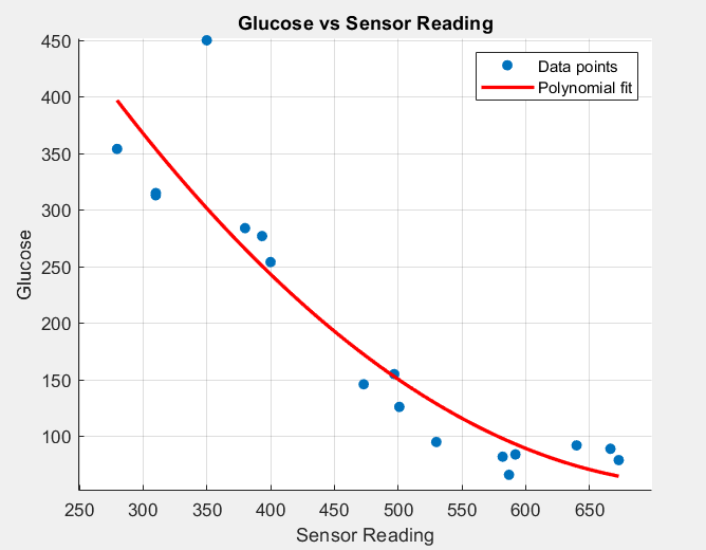

Figure7-1:Glucose vs Sensor Reading

NIR sensor reading(x)

Glucose reading(y)

$y = 0.0015845x^2 + -2.354x + 931.3579$

Microstrip resonator results:

Since the electromagnetic field of the resonators is changed by placing a material with a relative permittivity greater than 1 near them, the expectation for the toroidal resonator and the CCSR is to see a change in their responses when blood glucose levels change. Changes in $S21$ and $S11$ for the resonators are examined in both simulations (CST) and measurements To determine variations with changes in glucose concentrations, as shown in Figure 7.2, measurements are performed using a vector network analyzer (VNA).

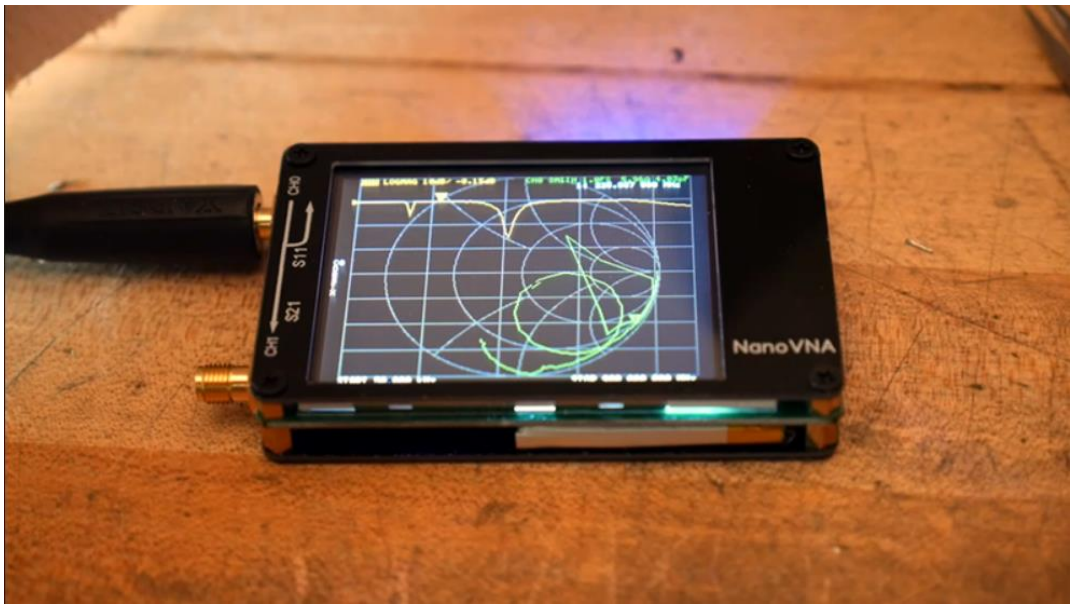

Figure 7.2: vector network analyzer (VNA)

1. CSRR-based sensor:

To validate the simulated result, the proposed structure was fabricated, and the structure's fabrication is depicted in Fig. 7-2. As the figure shows, the resonator is connected to two subminiature version-A (SMA) connectors via a feed transmission line. Later, the SMA connectors were connected to the Vector Network Analyzer (VNA) to carry out the measurements. The reflection coefficient response, S11, of the resonator was observed through the VNA, as depicted in Figure7-2. Samples were obtained using the finger prick technique. The primary point of reference for assessing glucose levels was glucometer. Next, blood glucose levels were assessed through the designed metamaterial resonator sensor.

In the following pictures, the sensor reading for a healthy person with diabetes was examined with the traditional device, and his result was 89 mg/dL.

Figure 7.3(a): The reflection coefficients of the microwave sensor

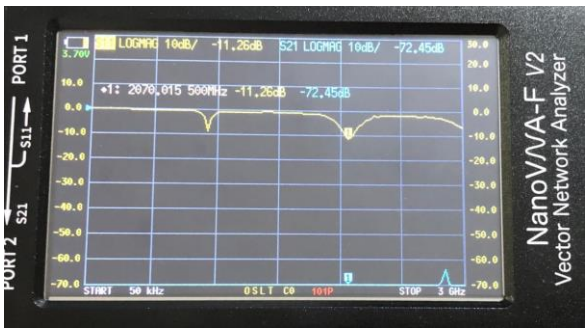

Figure 7.3(a): The reflection coefficients of the microwave sensor

Figure 7.4: Measured transmission response |S21|

2. Prototype Sensors:

The steps were repeated as for the CSRR-based sensor, but with one change: the resonator was connected to a single small type A (SMA) connector across the feeder transmission line and tested with s11 then with s21.

In the following pictures, the sensor reading is for a diabetic patient who was examined with the traditional device, and his result was 293 mg/dL.

Figure 7.5: Measured transmission response |S21|

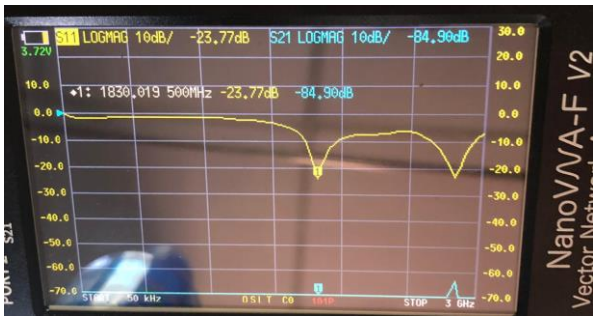

Figure 7.6: The reflection coefficients of the microwave sensor

In the following pictures, the sensor reading for a healthy person with diabetes was examined with the traditional device, and his result was 89 mg/dL.

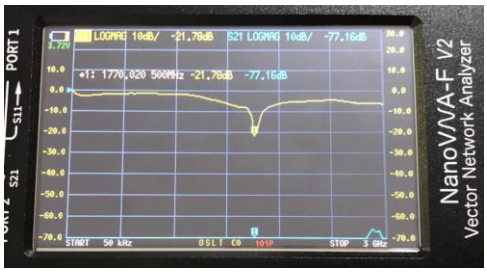

Figure 7.7: The reflection coefficients of the microwave sensor

Figure 7.8: Measured transmission response |S21|

3. Stepped Impedance Resonator Sensor:

The steps were repeated as for the CSRR-based sensor, but with one change: the resonator was connected to a single small type A (SMA) connector across the feeder transmission line and tested with s11 then with s21.

In the following pictures, the sensor reading is for a diabetic patient who was examined with the traditional device, and his result was **293 mg/dL.**

Figure 7.9: The reflection coefficients of the microwave sensor

Figure 7.10: The transmission coefficients of the microwave sensor

In the following pictures, the sensor reading for a healthy person with diabetes was examined with the traditional device, and his result was 89 mg/dL.

Figure 7.11: The transmission coefficients of the microwave sensor

Figure 7.12: The reflection coefficients of the microwave sensor

The final results of the 3 resonators:

A 3 low-cost microwave sensors of high sensitivity was presented for monitoring the blood glucose levels of diabetes.Microwave sensors have been investigated by taking a reading of an infected person and comparing the result to a healthy person.In the three designs, the results for transmission S21 were unclear, unlike the results for The reflection coefficient S11, which showed a clear response to changing the glucose concentration in the sugar.

References:

- Hina, A. and Saadeh, W., 2022. Noninvasive blood glucose monitoring systems using near-infrared technology—A review. *Sensors*, *22*(13), p.4855.
- Afshari, N., Hashemi, S.M. and Geran, F., 2023. Sensitivity evaluation of miniature microstrip line-based sensors using multiple sensing parameters for non-invasive blood glucose monitoring. *IET Microwaves, Antennas & Propagation*, *17*(11), pp.872-886.
- Shokrekhodaei, M., Cistola, D.P., Roberts, R.C. and Quinones, S., 2021. Non-invasive glucose monitoring using optical sensor and machine learning techniques for diabetes applications. *IEEE Access*, *9*, pp.73029-73045.
- Khoshhesab, Z.M., 2012. Reflectance IR spectroscopy. *Infrared spectroscopy-Materials science, engineering and technology*, *11*, pp.233-244.
- Science Mission Directorate. "Infrared Waves" NASA Science. 2010. National Aeronautics and Space Administration. *[insert date - e.g. 10 Aug. 2016]* http://science.nasa.gov /ems/07_infraredwaves
- Hina A, Saadeh W. Noninvasive Blood Glucose Monitoring Systems Using Near-Infrared Technology-A Review. Sensors (Basel). 2022 Jun 27;22(13):4855. doi: 10.3390/s22134855. PMID: 35808352; PMCID: PMC9268854.
- Jain, P., Maddila, R. and Joshi, A.M., 2019. A precise non-invasive blood glucose measurement system using NIR spectroscopy and Huber's regression model. *Optical and Quantum Electronics*, *51*(2), p.51.
- Tran, N.T. and Fukuzawa, M., 2020. A portable spectrometric system for quantitative prediction of the soluble solids content of apples with a pre-calibrated multispectral sensor chipset. *Sensors*, *20*(20), p.5883.
- ShahmohammadiMehrjardi, M., 2020. *Noninvasive Blood Glucose Measurement Using Microwave Resonators* (Doctoral dissertation, California State University, Northridge).
- Bin Yunos, M.F.A.; Nordin, A.N.; Zainuddin, A.; Khan, S. Modeling and development of radio frequency planar interdigital electrode sensors. Bull. Electr. Eng. Inform. **2019**, 8, 978–984.